UNIVERSITÀ DEL PIEMONTE ORIENTALE

School of Medicine
Department of Health and Sciences
Master's Degree in Medical Biotechnology

Thesis

Comparative Evaluation of Cell Seeding Strategies on 3D-Printed PLA Scaffolds Using Image Analysis and Machine Learning

Firmato digitalmente da Andrea Cochis
Data: 25.09.2025 13:05:03 CEST
Organizzazione: UNIVERSITA' DEGLI STUDI DEL PIEMONTE ORIENTALE/01943490027

Supervisor:

Professor Andrea Cochis

Co-Supervisor:

Professor Lia Rimondini

Candidate:

Negin Ejtehadi

Matricula: 20053431

Firmato digitalmente da Lia Rimondini
Data: 26.09.2025 07:28:01 CEST
Organizzazione: UNIVERSITA' DEGLI STUDI DEL PIEMONTE ORIENTALE/01943490027

The Academic Year 2024-2025

Acknowledgment

I would like to express my deepest gratitude to Prof. Andrea Cochis and Professor Lia Rimondini for his invaluable guidance, patience, and support during this thesis. My sincere thanks also go to Dr. Mauro Nascimben and Dr. Farah Daou for their constructive feedback and encouragement throughout this journey.

I am deeply thankful to my parents for their unconditional love and sacrifices, and to my beloved sister for her endless support. I am also sincerely grateful to my friends, especially Sara, Farnoush, and Parinaz, for their kindness and motivation.

Table of Contents

ABSTRACT **4**

1.INTRODUCTION **5**

1.1. 3D-PRINTING OF BIOMATERIALS **6**

1.2. PLA SCAFFOLDS **8**

1.3. COLLAGEN **8**

1.4. ALGINATE **9**

1.5. APPLICATIONS OF MACHINE LEARNING IN BIOMEDICAL RESEARCH **9**

1.5.1. Orange Data Mining[45]: Visual ML for Biomedical Tasks 10
1.5.2. Python[47]: A Flexible ML Ecosystem for Biomedicine 11
1.5.3. Machine Learning in Tissue Engineering: Applications and Examples 12
1.5.4. Ease of Use vs. Flexibility: Orange and Python for Researchers 15

1.6. AIMS OF THE CURRENT STUDY **16**

2.MATERIALS AND METHODS **18**

2.1. DESIGN, FABRICATION, AND EVALUATION OF BIOMIMETIC PLA SCAFFOLDS USING 3D PRINTING **19**

2.2. PERFUSION BIOREACTOR WITH A PEMF STIMULATOR AND A PARALLEL PROCESSING SYSTEM **19**

2.3. EVALUATION AND PREPARATION OF TRABECULAR BONE-LIKE TISSUE **19**

2.4. CELL CULTURE UNDER TWO DISTINCT CIRCUMSTANCES **20**

2.5. CELL VIABILITY ASSAY **21**

2.6. MACHINE LEARNING ANALYSIS **22**

3.RESULTS **23**

3.1. EXPLORATORY DATA ANALYSIS (EDA) **24**

3.1.1. Key findings: 25
3.1.2. Scientific insights: 26

3.2. STATISTICAL ANALYSIS – ANOVA **27**

3.2.1. Results of One-Way ANOVA Statistical Analysis 28
3.3. Feature Engineering and Machine Learning 32

3.5. MODEL INTERPRETATION AND EXPLAINABILITY **39**

3.5.1. Feature Importance 39
3.5.2. SHAP (SHapley Additive Explanations) 39
3.5.3. Conclusion of Model Interpretation and Explain-ability: 40

3.6. SUMMARY OF RESULT'S SECTION **40**

4.DISCUSSION **42**

5.CONCLUSION **52**

6.SUMMARY **59**

7.BIBLIOGRAPHY **60**

APPENDIX **68**

Abstract

Three-dimensional (3D) printed polylactic acid (PLA) scaffolds with trabecular bone-mimicked architecture have proven to be promising preclinical in vitro models for tissue engineering due to their biocompatibility, biodegradability, and structural tunability. Uniform and viable cell distribution throughout the pore network of the scaffold is one of the major challenges involved in scaffold-based cell culture.

This study presents a comparative investigation of three cell seeding methods, conventional suspension in culture medium, seeding in 2% alginate hydrogel, and seeding in 0.5% collagen hydrogel, on 3D-printed PLA scaffolds under static culture conditions. Although both static and perfusion-based dynamic culture environments were included in the experimental setup, the current analysis focuses solely on static samples. The high-resolution imaging was captured using the confocal microscope THUNDER Imager, and quantitative image analysis was performed for the detection of morphological and intensity-based cellular features. Through the use of machine learning techniques like Random Forest classification and SHAP analysis, the most discriminant features were identified. The most significant features to discriminate between seeding groups were found to be minimum fluorescence intensity and spatial centroid along the Z-axis.

The findings indicate that hydrogel-based methods, particularly collagen, improved cell distribution homogeneity and viability compared to traditional media-based suspension. Cells cultured in the pure medium underwent higher staining intensity variability and space localization, in comparison.

These results demonstrate the essential role of seeding materials on cell-scaffold interaction optimization in static conditions. Quantitative image-based analysis coupled with machine learning constitutes an unbiased and powerful method for scaffold performance evaluation, which allows for more precise engineering of biomimetic substrates for tissue regeneration.

1.Introduction

Background:

The development of novel scaffolds replicating biological and mechanical properties of native tissue are currently attracting attentions.[1–3] These scaffolds must possess a proper micro/nanostructure to facilitate the transportation of nutrients and metabolic waste to allow the scaffolds to have desirable mechanical, bioactivity, osteoconductivity, and osteoinductivity properties.[1,2] Hitherto, several fabrication techniques have been introduced to fulfill these specifications, most of which are related to an efficient surface chemistry method.[3] Three-dimensional porous scaffolds with biocompatibility, biodegradability, and homogeneity, produced by methods such as electrospinning, inverse opal, solid free-form fabrication, and freeze-drying.[4–6] These scaffolds, designed for triggering cellular activity and promoting bone formation, have been widely focused on in tissue engineering. Owing to this, tissue engineering is highly sought after, as their biological and mechanical properties need to be nearly similar to host tissue.[6,7] The microstructure of a perfect scaffold should also have a three-dimensional dense capillary network; this will help in the elimination of waste products from the tissue and also allow nutrients and oxygen to diffuse into the tissue.[8] In previous research by Muschler et al., they observed an indirect correlation between scaffold porosity and hypoxia and necrosis rates within host tissue. Hence, the most desirable scaffold is one which is completely porous with interconnected pore architectures to facilitate the exchange of vital biological components and flows.[9]

1.1. 3D-Printing of Biomaterials

In recent decades, the ability of computer-aided additive manufacturing technologies to generate 3D micro-nanostructures with interconnected structures that are highly porous and well-defined has become a popular topic.[10,11] Examples of these advanced fabrication processes include stereolithography, selective laser sintering, 3D bioprinting, and fused deposition modeling (FDM), all capable of generating patient-specific, intricately interconnected porous 3D structures composed of single or multiple materials.[12,13] It is imperative to select the appropriate materials, design the internal structure, and evaluate the mechanical properties of the results when selecting an additive manufacturing technique for tissue engineering applications.[14] Fused deposition

modeling (FDM) is becoming more prevalent in this context due to its ability to slice the microstructure with precision, thereby reproducing consistent patterns.[15,16] The morphology and mechanical properties of the scaffolds can be influenced by the modification of the distance between adjacent strands on a single layer or the orientation of two consecutive layers, which is possible with FDM. In turn, these factors influence the biological properties of the scaffolds, including cell viability, proliferation, and differentiation.[17]

Furthermore, the predictable functionality and cell distribution can be managed through the use of scaffolds with a consistent pattern. In contrast to 30% and 70% groups, Xia et al. discovered that 3D-printed hydrogel scaffolds for cartilage regeneration exhibited a more uniform distribution and a higher chondrocyte seeding efficiency with 50% infill density.[18] Furthermore, Markovic et al. discovered that 3D printed polylactic acid (PLA) scaffolds treated with methacrylamide-modified gelatin exhibited uniform cell dispersion and high inoculation efficiency when employed as hybrid substrates for pre-osteoblast cells derived from the mouse calvaria.[19] Kumar et al. discovered that an interconnected pore network with predefined architecture and pore size promotes vascularization in porous-structured scaffolds and ensures the long-term success of implants, in contrast to the distorted path that could potentially impede the development of blood capillaries and the flow of vital nutrients and oxygen throughout tissue remodelling.[20] The scaffold designed for tissue engineering applications must be considered as a temporary substitute for the natural extracellular matrix (ECM) of the tissue that is to be regenerated, closely approximating its microarchitecture. Although the inner morphology may be susceptible to spatial control, it should also undergo a comprehensive revision. Instead of the regular and repeated assembly of essential components like collagen or elastin, it is crucial to imitate the pattern of the extracellular matrix (ECM), which is frequently characterized by a complex structure, in order to facilitate optimal integration within the scaffold and the adjacent biological tissue to be repaired.[21–25]

Therefore, it is essential to utilize a manufacturing method that enables comprehensive control over the fabrication processes and the manufactured scaffold, together with the ability to attain repeatability over several layers. In addition, the morphology of the scaffold is closely correlated with the cell response, which underscores the significance of scaffold

design.[26] Traditional fabrication techniques, such as freeze-drying and solvent casting/salt leaching, exhibit insufficient controllability and accuracy for scaffold production. Conversely, Fused Deposition Modeling (FDM) is a technique that is consistent and reproducible, enabling the precise control and modification of scaffold architecture.[27,28]

1.2. PLA Scaffolds

A diverse range of materials has been extensively utilized in the past for scaffold fabrication. These comprise ceramics, synthetic materials, and natural fibers such as collagen, alginate, and chitosan.[29–31] Utilizing synthetic materials allows for enhanced control over the scaffold's physical, chemical, mechanical, and degradation properties. Furthermore, the process of fabrication may be optimized, enabling enhanced regulation of characteristics like as porosity, anisotropies, morphologies, and cell attachment or migration. The risk of toxicity and inflammatory responses remains a challenge in tissue engineering when utilizing synthetic materials for scaffold fabrication. Polymers such as polyglycolic acid (PGA), polylactic acid (PLA), and their hybrid, polylactic co-glycolic acid (PLGA), are the predominant materials employed. These polymers often undergo degradation by random hydrolysis of their ester linkages; for example, the degradation of PLA yields lactic acid, a biocompatible compound as it naturally occurs in the human body.[29] Therefore, a new method for generating and deploying optimal scaffolds that are entirely compatible with target tissues may be achievable by combining these polymers with natural biopolymers.

1.3. Collagen

Collagen is a very popular biomaterial for tissue engineering researchers due to a number of reasons. These include its high hydrophilicity, low antigenicity, and good cellular biocompatibility, e.g., cell attachment and proliferation, which are facilitated by the bonding between collagen's RGD domains and integrin receptors in cell membranes.[32,33] It has found its way into a variety of products, e.g., haemostatic pads, drug delivery systems, skin, cartilage, and bone, because it makes up 32% of the volume of bone and 89% of the organic matrix.[34,35] However, its applications have been constrained by its

undesirable mechanical properties, high cost, and poor processing ability in terms of microstructural control.[36]

1.4. Alginate

Alginate, a naturally occurring anionic polysaccharide, is a widely utilized biopolymer in tissue engineering research.[37] The material is beneficial for studies pertaining to muscle/smooth muscle cells, bone, aortic valve leaflet interstitial cells, cell encapsulation, wound dressing, tissue regeneration, and pharmaceutical application, cartilage, and analogous tissues due to its accessibility, affordability, excellent biocompatibility, and little cytotoxicity.[37] It possesses specific characteristics, including the capacity to establish an inert hydrodynamic environment, undergo sol-gel transformation under moderate circumstances, exhibit tunable porosity for adjustable molecular transport, biodegrade in physiological settings, and structural resemblance to the extracellular matrix.[38–41] Since alginate lacks the bioligands necessary for mammalian cell adhesion, which results in limited bioactivity, it is imperative to develop customized composites of alginate and other hydrogels/polymers to improve cell responses and achieve tissue-specific features for an optimal scaffold.[42]

1.5. Applications of Machine Learning in Biomedical Research

Machine learning (ML) is now standard practice in biomedical research for tasks like data visualization, feature selection, model training, and outcome prediction. Researchers use ML to explore complex data sets (e.g. genomic profiles or imaging data), identify significant features (e.g. predictive genes or biomarkers), train models to classify or predict clinical outcomes, and ultimately use those models to make predictions on new data for diagnosis or therapy guidance.[43] Both Orange (the Orange Data Mining platform) and Python (with its rich ML libraries) are widely used tools that facilitate these tasks. They tackle the challenges from different angles: Orange provides a graphical, no-code environment for simple discovery, while Python offers a coding-based ecosystem with strong libraries for deep customization. Below, we discuss how each is applied in biomedical ML and then highlight examples in tissue engineering, including 3D-printed

PLA scaffolds, printing parameter optimization, and improving cell seeding and biological outcomes.[44]

1.5.1. Orange Data Mining[45]: Visual ML for Biomedical Tasks

Orange is an open-source visual programming platform for data mining and machine learning. It allows researchers to build analysis workflows by dragging-and-dropping components (widgets) on a canvas – no coding needed. Users can load datasets, preprocess them, perform analysis, and visualize results by connecting these widgets in a pipeline. This makes Orange extremely accessible to clinicians, biologists, and other non-programmers. For example, Orange provides interactive data visualization widgets to explore distributions, box plots, scatter plots, and also advanced methods such as hierarchical clustering, heatmaps, multidimensional scaling (MDS), t-SNE, and PCA projections. Such tools enable biomedical scientists to intuitively examine their data (e.g. gene expression levels, patient measurements, etc.) and detect patterns without writing code.

Orange also supports feature selection through widgets such as Rank, which scores and ranks variables by how informative they are for predicting a given outcome (Orange Data Mining - Feature Selection.[46] This is especially useful in biomedical contexts (like genomics or imaging) where one might want to find the top genes or image features correlating with a disease or treatment outcome. The platform includes various modeling widgets (for regression, classification, clustering, etc.), so users can train models (e.g. a decision tree or random forest) by simply configuring a widget and connecting it to the data source. Predictions can then be made by feeding new data into the trained model widget, and evaluation widgets can assess performance (accuracy, ROC curves, etc.), all without coding.

Another strength of Orange is its extensibility and specialized add-ons for biomedical data. There are extensions for text mining, network analysis, and even domain-specific data types like time series, survival analysis, spectra, and gene expression data. This means a researcher can, for instance, plug in a gene expression dataset (perhaps via GEO or TCGA data import widgets) and use Orange's bioinformatics add-ons to perform clustering or differential expression analysis visually. Orange's design has proven valuable in education and research: it is used in universities and workshops to teach data

science concepts, allowing students and scientists to learn by hands-on exploration rather than programming. This ease of use lowers the barrier for domain experts to apply ML on their own data. At the same time, Orange is built on a powerful Python backbone (NumPy arrays are its internal data structure), and it's open-source with the option to add new functionalities in Python. This means advanced users can extend it or integrate custom algorithms, bridging the gap between simple UI-driven analysis and the full flexibility of Python.

1.5.2. Python[47]: A Flexible ML Ecosystem for Biomedicine

Python is now the language of choice for machine learning in engineering and science, including biomedical science. It's due to the strong ecosystem of libraries and frameworks that exist to offer support with all stages of the ML pipeline. With Python, data scientists and engineers can write custom data processing and leverage libraries like Pandas to process biomedical datasets (patient data, omics data), access scikit-learn to leverage traditional ML algorithms (classification, regression, clustering, etc.), and connect into deep learning systems (like TensorFlow or PyTorch) for more sophisticated use cases like image recognition or sequence modeling. This flexibiliy allows Python users to tailor models extremely accurately to their problem. For example, while researching 3D-printed scaffold materials, scientists used Python to organize experimental data into Pandas data frames, feature normalization, and subsequently train ML models (Leveraging Machine Learning for Optimized Mechanical Properties and 3D Printing of PLA/cHAP for Bone Implant).[48] They experimented with various algorithms and performed hyperparameter tuning using scikit-learn's API to gain the optimal predictive performance. Python's extensive library support enables researchers to use the newest techniques or integrate tools domain-specific (e.g., employing OpenCV for computer vision examination of microscopy images, or Biopython for sequence analysis) that may not be part of out-of-the-box GUI packages.

In biomedical applications, Python has been used to anything from predicting the outcome of disease (e.g., labeling tumors as benign or malignant given diagnostic data) to biomedical image analysis (deep neural networks on pathology slides or MRI scans).[49] Perhaps the language's flexibility is best seen in its use in tissue engineering research: ML with a Python backend can incorporate specially designed algorithms like XGBoost

(extreme gradient boosting) or neural networks to output high accuracy on complex prediction tasks. In fact, in a recent study of 3D-printed bone scaffolds made of PLA, investigators integrated ML algorithms (XGBoost and AdaBoost) into their Python workflow to predict mechanical properties of novel composite scaffolds.[48] The models achieved excellent predictive accuracy (R^2 ≈ 0.91 for compressive strength and 0.88 for tensile strength) and demonstrated that a data-driven approach could "optimize material properties autonomously," greatly speeding up materials development.[48] The authors noted that using such Python-based ensemble models streamlined the material design process and significantly reduced the need for extensive and costly experimental trials.[48] This example shows how the flexibility of Python allows scientists to write complex ML techniques (beyond the reach of a point-and-click tool) and push the state-of-the-art in biomedical engineering.

1.5.3. Machine Learning in Tissue Engineering: Applications and Examples

Tissue engineering is a multidisciplinary field where ML is increasingly being applied to improve the design and outcomes of engineered tissues. Key challenges in tissue engineering include designing optimal scaffolds, choosing the right biomaterial formulations, tuning 3D printing parameters, and enhancing cell seeding and growth conditions. ML can assist in all these areas by learning from experimental data and guiding decisions. A review in 2024 enumerated some of the primary fields of application of ML in tissue engineering as the optimization of bioprinting and scaffold design techniques, predicting material–cell interactions, optimization of drug delivery systems, analysis of images of biological structures, and simulation of the in vivo behavior of scaffolds.[49] Below, we highlight a few examples – particularly focusing on 3D-printed PLA scaffolds and related tasks – to illustrate how Orange and Python-based ML have been used in this domain.

- **3D Printing Parameter Optimization:** Optimizing 3D printing parameters for scaffolds is another important application of ML in tissue engineering. For instance, Conev et al. (2020) developed an ML-based approach to propose the right print conditions for new scaffold materials.[50] In the production of scaffolds, finding the correct print settings (speed, pressure, temperature, etc.) for a specific material has long required extensive

trial-and-error. In this study, we used Orange/Python-based data analysis to train machine learning models (specifically, Random Forest classifiers/regressors) that distinguished low-quality prints from high-quality prints based on the input printing parameters and material composition.[50] The ML model takes parameters like material mix, printer settings, and layer information, and predicts whether the resulting scaffold will be of acceptable quality. They reported encouraging results: the Random Forest models correctly labeled most of the test printing settings as "high" or "low" quality, whereas a linear model was unable to reliably differentiate print quality.[50] This demonstrates that ML is able to discern the complex, nonlinear relationships between print settings and print output. Such a tool effectively acts as a smart guide for experimenters – it can suggest which combinations of parameters are likely to yield good scaffolds, thereby reducing the number of experimental iterations needed to achieve a functional scaffold. Experts note that this approach is transformative, since the ultimate problem in bioprinting is finding the best design and printing parameters to achieve target geometry, mechanical strength, and biological function.[51] Integrating ML as in the above example helps address this problem by screening for the best print settings (e.g. nozzle speed, layer thickness, etc.) to maximize quality, greatly cutting down laborious experimentation.[51]

- **Machine learning prediction of Scaffold Performance and Properties:** Machine learning is also used to predict the performance of different scaffold compositions or designs, which would enable scaffold properties to be designed as optimal. We had mentioned earlier about the work wherein PLA scaffolds reinforced with hydroxyapatite (cHAP) were investigated using Python ML techniques. In that work, researchers varied the composition (pure PLA vs. PLA with 7.5% or 10% cHAP) and measured mechanical properties (like compressive and tensile strength). By training an XGBoost regression model on the experimental data, they could accurately predict the strength of new scaffold compositions without needing to fabricate and test every variant.[48] The models attained high accuracy ($R^2 > 0.87$) in predicting mechanical outcomes, indicating the ML learned the mapping between scaffold parameters and performance.[48] Perhaps more importantly, this ML-driven approach allowed them to identify optimal composition and printing parameters that improve scaffold strength, while saving considerable time and resources. As the authors describe, collective methods like

AdaBoost and XGBoost proved to be "powerful tool[s] in predicting the mechanical properties of the composites," making design easy and significantly removing the need for large-scale experimental trials.[48] In practical terms, this means engineers can use the trained model to virtually “test” many combinations of material and print settings, and focus only on the most promising ones for real-world fabrication. Such predictive modeling is especially valuable in tissue engineering, where material testing is time-consuming and expensive. It makes the field move towards data-driven scaffold design, with the aid of AI to enable human experts to design scaffolds with bespoke mechanical and biological properties more efficiently.[48]

- **Improving Cell Seeding and Biological Outcomes:** Beyond mechanical properties, ML is also helping optimize the biological performance of tissue-engineered constructs. One concern in scaffold-based tissue engineering is ensuring that cells can attach, survive, and proliferate throughout the scaffold (since a scaffold that prints well is only useful if it also supports tissue growth). Researchers have started applying ML models to relate fabrication parameters or scaffold features to cell viability and tissue outcomes. For example, a recent approach used several ML algorithms (random forests, k-nearest neighbors, ridge regression, neural networks) to analyze how bioprinting conditions affect cell viability in a 3D bioprinted scaffold using a light-curable bio-ink.[51] By training on data that included variables like ultraviolet (UV) light intensity and exposure time (critical factors for photocrosslinking the scaffold and potentially harmful to cells), the models could “determine cell viability” under different conditions.[51] This revealed the impact of each parameter – e.g., excessive UV exposure could substantially reduce live cell percentages – and allowed print settings to be determined that result in high cell viability. More broadly, ML can be combined with biological feedback (attachment rates, proliferation, differentiation markers, etc.) into the optimization loop for scaffold design. In the future, we can envision using Orange or Python ML libraries to predict the optimal pore size, scaffold geometry, or seeding protocol that provides us with the most appropriate cell distribution and growth and, by learning from previous experiments (and even simulations), such models would teach bioengineers how to architect scaffolds that not only meet mechanical specifications but also achieve healthy tissue growth. Indeed, early studies and reviews suggest that machine learning, combined with advanced

biofabrication, can help strike the right balance between scaffold printability and cell viability/function, thus improving the fidelity of complex bioprinted tissues.[51] The end goal is to use ML to reduce trial-and-error in both the fabrication stage and the biological validation stage, accelerating progress toward scaffolds and tissue constructs that function well in clinical settings.[51]

Notably, while many of these cutting-edge tissue engineering studies implement ML via custom Python code, the insights and workflows can be made accessible through tools like Orange as well. A biomedical researcher could use Orange to visualize relationships, for example, plotting how cell viability varies with scaffold pore size and perform basic predictive modeling on a small dataset. This ease of exploration complements the heavier Python-driven modeling used in large-scale studies.

1.5.4. Ease of Use vs. Flexibility: Orange and Python for Researchers

Orange and Python each have distinct advantages, and the choice often depends on the user's background and project needs:

- **Orange – Intuitive Analytics:** Orange is appropriate for researchers who have no programming skills or who prefer to see the whole thing at once. Its drag-and-drop interface diminishes ML as a barrier to entry, under which domain professionals are able to carry out sophisticated analysis with minimal training. "No coding required" is one of its unstated philosophies[45], workflows are built by dragging and dropping components into position, so the process is transparent and traceable. This is especially convenient when working collaboratively, as Orange's visual workflows can be shared and discussed with ease. Non-programmers can load data and immediately start exploring patterns or training models. For example, a biologist could import experimental data (e.g. gene expression or scaffold testing results) and quickly identify important features or try out a classifier, all within a couple of hours of learning Orange. Orange also provides direct graphical feedback (plots, charts) at each stage, which is great for developing intuition. Orange's ease of use has some disadvantages, however: users are more or less limited to the provided widgets and installed algorithms. While many standard methods are covered, quite specialized analysis or bleeding-edge model designs may not be included

in Orange's GUI. In those cases, one would need to write Python code or create a novel Orange widget.[45]

- **Python – Developer's Power Tool:** Python, on the other hand, offers unmatched power and flexibility for individuals who are at ease with coding. In Python, one has full control over modifying each step in data analysis – from data preprocessing to model architecture designing – which is critical for cutting-edge research. The Python ecosystem (NumPy, Pandas, scikit-learn, PyTorch, etc.) is continually growing, often outpacing what GUI tools provide. Developers can develop new algorithms, handle big data (using libraries like Dask for parallel computing), and add ML models to pipelines or apps. These use cases make Python a first choice for projects that need bespoke solutions or high-level computations – for example, training a deep neural network on a thousand medical images, or finding the optimal scaffold structure with a genetic algorithm. The trade-off is that Python has a steeper learning curve. Researchers need to write and debug code, which requires coding knowledge and time. Yet, for those who invest in it, Python provides fine-grained control and access to state-of-the-art methods in machine learning and AI. It enables reproducible research through scripting and version control, and it's the language in which most new ML developments (and many biomedical data science libraries) are released. In short, Python empowers developers to push the boundaries of biomedical ML, at the cost of requiring programming expertise.[47]

1.6. Aims of the current study

Many researchers in the field of tissue engineering are interested in using AI, and more especially Machine Learning, to find the best printing settings for biomaterials and to make them more printable.[50,52–54] Machine learning may examine underlying behaviors inside a dataset to forecast future outcomes. In this case, it could optimize the printing parameters of scaffolds to improve their structural properties, printability, and print quality.[55–57]

In the current study, we employed three-dimensional printed scaffolds composed of polylactic acid (PLA), designed with an architecture that closely resembles that of trabecular bone. Our objective was to identify a cell seeding strategy that would facilitate uniform cell distribution throughout the scaffold. Consequently, we evaluated three

distinct methodologies: suspension seeding utilizing cell culture media, a mixture of cells with 2% alginate, and a combination of cells with 0.5% collagen.

In this experiment, two distinct cell culture environments were employed: a static setting using an incubator with a cell culture plate, and a dynamic setting using a perfusion bioreactor that provides fluid shear stress. These conditions were applied to evaluate the performance of the three different cell seeding strategies. However, the current thesis focuses exclusively on the analysis of static culture conditions, while dynamic culture data were not included in this study.

Also, this study aims to acquire quantitative morphometric and positional attributes of the seeded cells from high-resolution images taken from the Leica THUNDER microscope. Machine learning algorithms are employed to further investigate three properties including scaffold colonization, vitality, and cell dispersion, in order to determine the most effective seeding strategy.

The ultimate objective of the study is to facilitate the development of superior bone tissue regeneration methods by elucidating the optimization of cell inoculation strategies and 3D-printed scaffold designs.

2.Materials and Methods

2.1. Design, fabrication, and evaluation of biomimetic PLA scaffolds using 3D printing

The current study is based on previous research by Pecci et al. for the design and fabrication of the 3D-printed scaffold[58]. They developed the CAD models for the scaffold with a customized script. The software generated a random 3D distribution of spheres, functioning as virtual porogens with a diameter of 600 µm. The scaffold had to be subtracted from a cylindrical cylinder of 10 mm in diameter and 5 mm in height. Upon their import into IdeaMaker (Raise3D Inc., Irvine, CA, USA), script files were then executed with a Z-slice of 0.25 mm resolution. Printing of subsequent scaffolds was carried out using PLA filament (FormFutura BV, The Netherlands) on a Raise 3D N2 printer (Raise3D Inc., Irvine, CA, USA) with nozzle temperature calibrated at 205 °C and build plate temperature at 60 °C. Bioactivity of scaffolds has been explored and assessed.59 Permeability of the scaffolds on average was 2.36 x 10-10 m².[60]

2.2. Perfusion bioreactor system

Although this thesis focuses exclusively on static culture conditions, a perfusion bioreactor system was also used in the broader experimental setup.[61] This system was previously established and designed for automated, parallelized direct perfusion culture. It consists of three 3D-printed culture chambers, each connected to an individual closed-loop hydraulic circuit (produced by Darwin Microfluidics in France). A dedicated control unit, equipped with a microcontroller board (Arduino Micro, Arduino, Italy), regulates medium flow through each circuit using a multichannel peristaltic pump. The perfusion mechanism provides continuous medium circulation and exposes the samples to fluid shear stress, which is known to enhance osteoblast proliferation and tissue development.[62,63]

2.3. Evaluation and preparation of trabecular bone-like tissue

The basal medium (BM) used in this investigation was low in glucose. In order to culture human telomerase reverse transcriptase (hTERT)-immortalized BM-MSCCs of clonal line

Y201, which had previously been developed by James et al.[64], the following conditions were used: a humidified atmosphere with 5% CO_2 at 37 ^oC; DMEM low glucose supplemented with 15% fetal bovine serum (FBS) from Gibco Thermo Fisher Scientific, Inc.; and 1% antibiotics (penicillin/streptomycin, Gibco Thermo Fisher Scientific, Inc.). Before each experiment, cells were passaged following enzymatic digestion with trypsin/ethylenediamine tetra-acetic acid (trypsin/EDTA, Gibco Thermo Fisher Scientific, Inc.) to achieve 80-90% confluency.

2.4. Cell culture under two distinct circumstances

At a density of 3×10^6 cells and a volume of 200 µL, a 6-well cell culture plate was used as a base for directly seeding cells onto PLA scaffolds, which were then placed in the PDMS holders of the automated bioreactor. This was done by either suspension seeding or by employing cell-releasing hydrogels. In order to seed the cells in suspension, 200 µL of BM was used; for cell-releasing 2 % alginate, 4 % (40 mg/mL) alginate solution was prepared using alginic acid sodium salt from brown algae (Medium viscosity, Merck, Italy), and then mixed in a 1:1 ratio with the cell suspension. For the 0.5 % collagen solution that released cells, 200 µL of 5 mg/mL PureCol EZ Gel solution (Merck, Italy) was used. Cell infiltration and adhesion were enabled by incubating the samples for 4 hours. The next step was to cover the samples with BM and let them incubate overnight after seeding with suspension seeding and cell-releasing 0.5% collagen. On the other hand, samples that were seeded with cell-releasing 2% alginate were incubated overnight in 150 µL of 0.2 M calcium chloride ($CaCl_2$) solution. After that, they were washed once with phosphate-buffered saline (PBS, 1×) to eliminate the $CaCl_2$ solution. After the samples were incubated overnight, they were cultured for 21 days in either static culture or direct perfusion. In static culture, the samples were kept in a cell culture plate and BM was changed every 3–4 days. In direct perfusion, the samples were placed in an automated perfusion bioreactor and put under unidirectional, direct perfusion at 0.3 mL/min with 50 mL of BM pumped from the reservoir. The medium was changed every 7 days. Each sample was examined three times (n = 3).

2.5. Cell viability assay

Utilizing the live/dead cell assay (LIVE/DEADTM Viability/Cytotoxicity Kit for mammalian cells, Invitrogen Life Technologies), the vitality of BM-MSCs that were seeded onto biomimetic PLA scaffolds using one of three different cell seeding procedures and grown under one of two different conditions was evaluated on day 21 of culturing. In short, after being taken out of the bioreactor's CCs, the samples were transferred to a 24-well cell culture plate, rinsed with 1× PBS, and then incubated in a BM containing 2 μM calcein-AM and 2 μM ethidium homodimer-1 (EthD-1). A fluorescent microscope (THUNDER Imager 3D Cell Culture, Leica Microsystems) was used to observe the green calcine AM staining living cells and the red EthD-1 staining dead cells after 15 minutes of incubation at 37 °C and 5% CO_2 atmosphere.

Leica THUNDER is a widefield fluorescence microscope built for high-speed, high-clarity imaging of 2D and 3D biological samples. Its claim to fame is its new Computational Clearing technology, where digital removal of out-of-focus blur from thick samples occurs in real-time, consequently, delivering image quality comparable to confocal systems but with the speed and sensitivity of widefield microscopy.[65,66]

By design, THUNDER is headed for live-cell imaging and dynamic biological processes. The system employs sensitive sCMOS cameras in tandem with high-power LED light sources to capture fast biological events at low phototoxicity. It is therefore ideal for time-lapse imaging of living cells, organoids, or tissue slices over long periods.

In summary, built-in environmental control (temperature, CO_2, and humidity control) also ensure stable live imaging conditions over long durations.[66,67]

THUNDER is also compatible with multi-channel fluorescence imaging, allowing the visualization of multiple fluorophores simultaneously or sequentially at high precision. THUNDER has a motorized stage and automated Z-stack capability to enable quick and reproducible volumetric (3D) dataset collection. Importantly, THUNDER performs real-time optical sectioning using its computational clearing algorithm, removing background haze while maintaining signal intensity, which is especially beneficial for thicker samples where traditional widefield images are limited.[65,67]

The system is fully automated and operated using Leica's intuitive LAS X software to enable advanced acquisition protocols such as time-lapse, multi-position scanning, and

multi-dimensional imaging (XYZT). The features make it very well-suited for high-content experiments between dishes, slides, or multiwell plates.[67]

Due to its rapidity, clarity, and automation, the THUNDER microscope is being used more and more in labs for tracking cells, imaging 3D cultures, analyzing tissue sections, and organ-on-chip studies. Its ability to produce sharp, high-contrast images at a fast and reliable rate makes the THUNDER microscope a powerhouse in modern fluorescence microscopy.

2.6. Machine Learning Analysis

Machine learning classification was performed using a Random Forest model. To ensure robust evaluation and avoid overfitting, the dataset was split into three sets: 60% for training, 20% for validation, and 20% as a held-out test set. 10-fold cross-validation was performed on the training and validation sets so that model performance could be tuned without exposing the test data.

All the analysis was done in Python (v3.10) using the scikit-learn library and Orange Software. The best model was then implemented on the hold-out test set. The performance of the models was evaluated by accuracy, F1-score, and area under the ROC curve (AUC). The three-stage test was done for the model generalizing effectively from the training data.

3.Results

3.1. Exploratory Data Analysis

In this section, the main goal was to investigate the overall structure of the dataset and identify the initial patterns as well as study the relationship between extracted particle-level characteristics. A thorough understanding of the pre-modeling phase data depends on this step. Histogram plots were used here to show the distribution of features among the three distinct cell seeding methods (Alginate, Collagen, and Medium) and to achieve the desired result. The scatter plots and Pearson correlation analysis were also used to investigate the relationship between significant variables.

The main results of this stage were insights into the variations in feature distributions across seeding techniques, relationships between features (e.g. volume vs. surface area or intensity), and the identification of features that are strongly or weakly correlated. These findings guided following choices on feature selection and modeling, thus providing a vital basis for efficient feature engineering and classification modeling in the next stages.

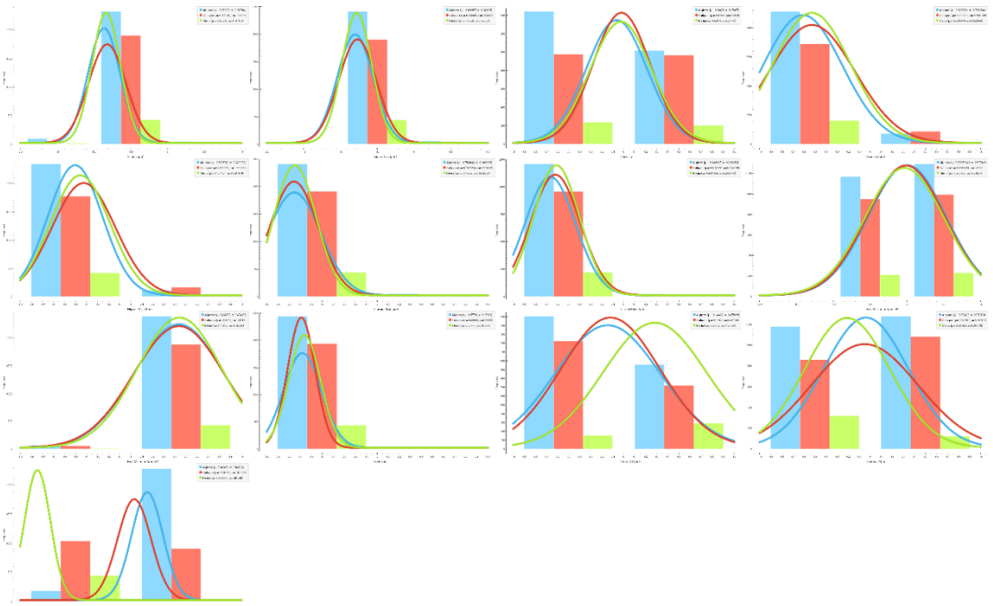


Figure 3.1. Histogram and kernel density estimation (KDE) plots of single-particle morphology recovered from PLA scaffolds seeded using three different protocols: alginate, collagen, and culture medium. Each subplot displays the distribution of one single particle-level feature obtained via image-based analysis. The parameters that are analyzed are: (Top row, left to right): Volume, Mean Intensity, Standard Deviation of Intensity, Area (Middle row, left to right): Circularity, Feret Max Diameter, Feret Min Diameter, Distance from Geometric Center (Bottom row, left to right): Solidity, Roundness, Aspect Ratio, Compactness.The results indicate that different methods of cell seeding alter the distribution of the particles' morphological characteristics inside the scaffold, and these variations may influence cell positioning, movement, and growth within the three-dimensional scaffold environment.

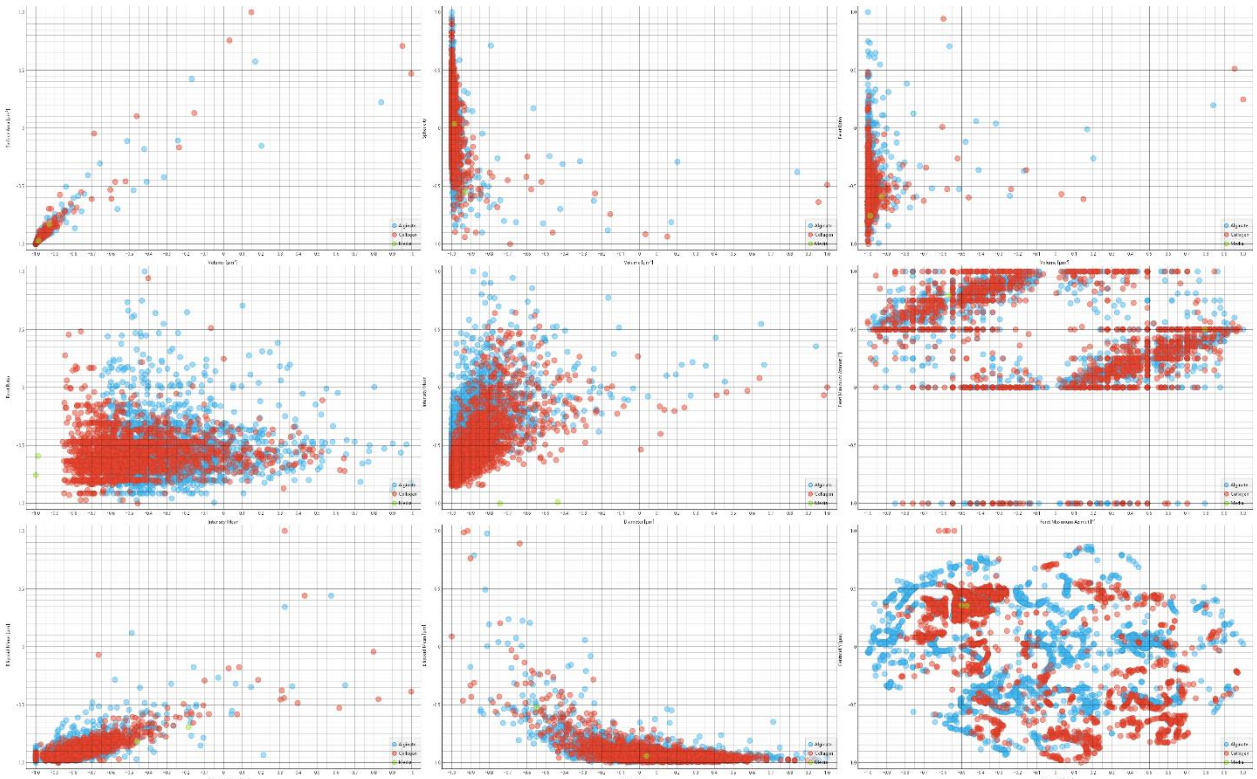


Figure 3.2. Scatter plots of single-particle morphological features retrieved from PLA scaffolds seeded by three different methods: alginate, collagen, and culture medium. This figure presents pairwise scatter plots of various quantitative parameters derived from image-based analysis of individual particles or cells. These are volume, surface area, sphericity, fluorescence intensity, diameter, centroid coordinates, ellipsoid dimensions, and inset angles. Every point is an individual object, and its color is the corresponding cell seeding procedure.

3.1.1. Key findings:

Based on the results in Figures 3.1 and 3.2, a high positive relationship between particle volume and surface area and between volume and sphericity is identified, which indicates that larger size particles are far from being spherical in shape. Additionally, unique patterns of clustering by seeding techniques are evident, indicating differences in cell distribution and morphology. Overlapping within certain feature spaces may also show similar biological or physical properties of the particles. Moreover, Ellipsoid and Feret-based shape descriptors enable the differentiation of seeding strategy morphological subtypes. Finally, centroid X and Y distributions indicate cell spatial dispersion on the scaffold surface.

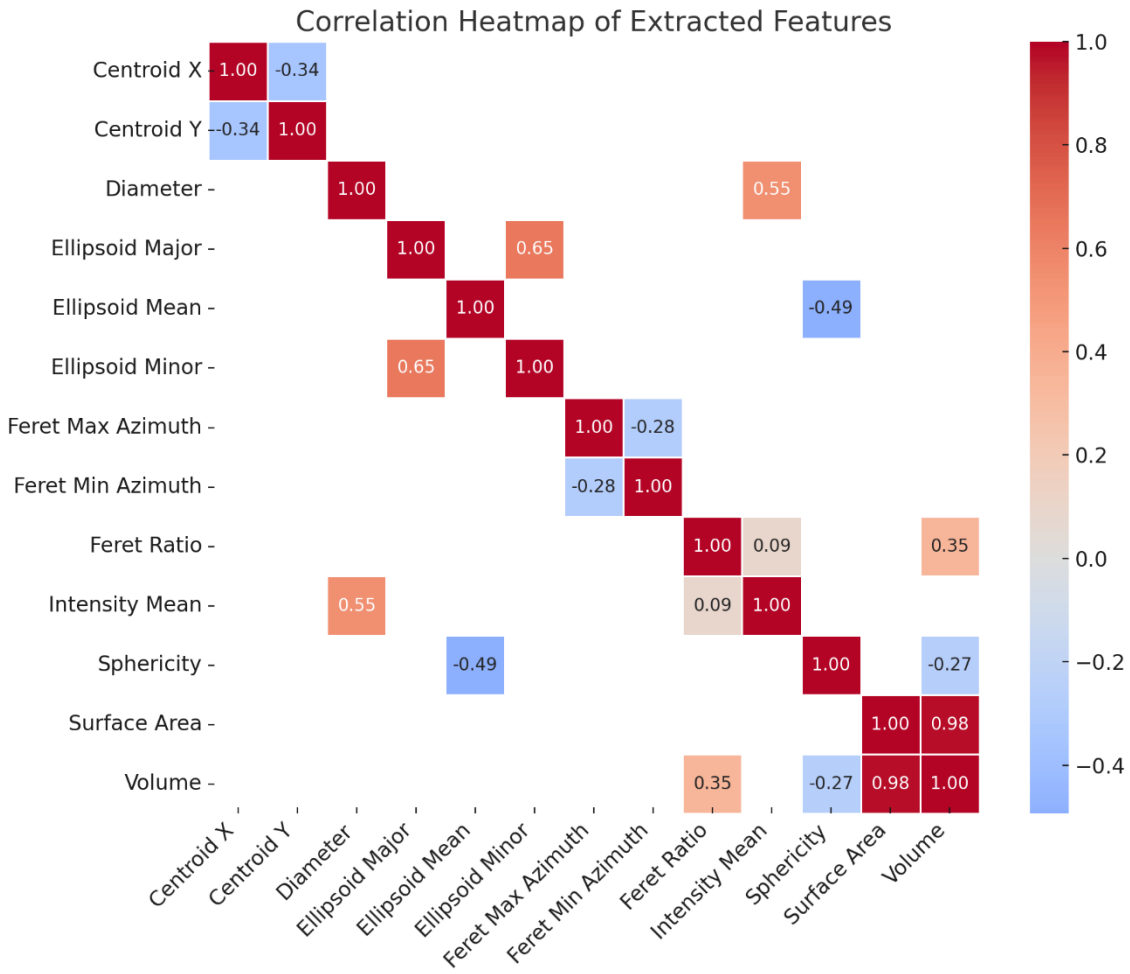


Figure 3.3 Histogram and kernel density estimation (KDE) plots of particle-level morphological features extracted from PLA scaffolds seeded by three different methods: alginate, collagen, and culture medium. Each subplot shows the distribution of one particle-level feature obtained from image-based analysis. The parameters examined are: (Top row, left to right): Volume, Mean Intensity, Std Dev Intensity, Area (Middle row, left to right): Circularity, Feret Max Diameter, Feret Min Diameter, Distance from Geometric Center (Bottom row, left to right): Solidity, Roundness, Aspect Ratio, Compactness.

3.1.2. Scientific insights:

In Fig. 3.3, KDE plots illustrate big differences in feature distributions by the seeding process with suggestions of multi-effects on morphology at the cell level. Scaffolds seeded in culture medium present broader and more dispersed feature ranges compared to scaffolds seeded using hydrogel techniques (alginate and collagen). Alginate-seeded scaffolds show higher circularity and coherence, while those seeded with collagen show larger dispersion of size parameters. These differences indicate that the choice of seeding method has a high potential to influence spatial arrangement and cell shape in cells in 3D-printed scaffolds.

3.2. Statistical Analysis – ANOVA

The goal in this phase was to check whether statistically significant particle-level feature changes existed between the three distinct cell-seeding protocols (Alginate, Collagen, and Medium). One-way analysis of variance (ANOVA) was used to conduct this for each attribute.

At least three independent groups are compared using one-way ANOVA to determine the mean of a continuous variable. The null hypothesis holds that all the group means are equal. If p-value < 0.05, i.e., at least one group is significantly different from others, then null hypothesis is rejected. This statistical study enabled us to find very dissimilar features between groups, which can perhaps serve as good predictors in future machine learning models.

Table 3.1. Statistical Analysis ANOVA

	Mean	Variance	Skewness	Kurtosis	F-statistic	p-value
Class	-0.8436	0.053587	2.904187	10.60523	19.01574	5.94E-09
Volume [µm³]	-0.8436	0.053587	2.904187	10.60524	19.01594	5.94E-09
Volume Filled [µm³]	-0.8436	0.053594	2.904554	10.60819	19.00704	5.99E-09
Convex Volume [µm³]	-0.88133	0.033914	3.459427	15.7748	9.743581	5.98E-05
Surface Area [µm²]	-0.78573	0.059908	2.616156	8.910783	9.577385	7.06E-05
Surface Area Filled [µm²]	-0.78574	0.059883	2.615341	8.906497	9.596613	6.93E-05
Convex Surface Area [µm²]	-0.80418	0.043199	2.400806	7.563627	14.25409	6.72E-07
Sphericity	-0.04317	0.07245	-0.01867	0.409962	15.48556	1.98E-07
Diameter [µm]	-0.56883	0.138768	1.136394	0.942234	31.04014	4.03E-14
Ellipsoid Major [µm]	-0.46826	0.071908	0.980111	1.567988	46.63739	8.68E-21
Ellipsoid Mean [µm]	-0.75079	0.051682	2.796881	11.30886	0.248569	0.779926
Ellipsoid Minor [µm]	-0.64095	0.051213	1.42904	2.738774	27.85019	9.42E-13
Feret Maximum [µm]	-0.44175	0.096244	1.044507	1.390052	42.80776	3.73E-19
Feret Maximum Azimut [°]	-0.0082	0.280319	-0.0629	-1.36073	1.061093	0.346158
Feret Maximum Elevation [°]	-0.12031	0.849379	0.258607	-1.92215	6.395558	0.001683
Feret Minimum [µm]	-0.55853	0.065793	1.343877	2.309716	25.4979	9.65E-12
Feret Minimum Azimut [°]	0.435224	0.163838	-0.91744	1.979577	0.035509	0.965115
Feret Minimum Elevation [°]	-0.32707	0.009429	1.818549	38.93796	0.504276	0.603974
Feret Ratio	-0.67898	0.022982	1.998153	9.225225	6.600602	0.001372
Centroid X [µm]	-0.09616	0.228935	0.218799	-1.01411	161.5453	1.22E-68
Centroid Y [µm]	-0.05839	0.183075	-0.16241	-1.08181	30.26301	8.68E-14
Centroid Z [µm]	-0.38073	0.204901	0.812744	0.067706	670.5521	9E-258
Bounds X [µm]	-0.86567	0.010872	3.819949	35.96745	4.468079	0.011517
Bounds Y [µm]	-0.84585	0.021133	3.204351	18.29687	0.446796	0.639701
Bounds Z [µm]	-0.44191	0.097457	1.035085	1.400816	45.88959	1.81E-20
Intensity Sum	-0.84838	0.049205	3.058486	11.59413	32.06245	1.47E-14
Intensity Mean	0.011169	0.096732	-1.63891	3.302622	8980.75	0
Intensity Standard Deviation	-0.58199	0.084212	1.592677	3.237819	31.92135	1.69E-14
Intensity Minimum	0.538871	0.245597	-2.60262	5.284312	1384417	0
Intensity Maximum	-0.1479	0.1101	0.450712	1.256765	1085.388	0

3.2.1. Results of One-Way ANOVA Statistical Analysis

One-way ANOVA was applied on all retrieved data in Table 3.1 to find particle characteristics that differ markedly across the three cell-seeding techniques (Alginate, Collagen, and Medium). Statistical significance was $p < 0.05$.

3.2.1.1. Features with Highly Significant Differences ($p < 0.001$):

These features showed strong and highly significant differences between groups:

Feature	P-Value
Centroid Z	9×10^{-258}
Intensity Mean	0
Intensity Maximum	0
Feret Maximum	3.73×10^{-19}
Ellipsoid Major	8.68×10^{-21}
Bounds Z	1.81×10^{-20}

These parameters are good candidates for classification modeling and could indicate different biological or structural behaviors depending on the seeding technique.

3.2.1.2. Features Without Significant Differences ($p > 0.05$):

The following features did not vary significantly between the groups. Therefore, they are far less probable to contribute with categorization in a meaningful way.

Feature	p-Value
Feret Maximum Azimuth	0.346
Feret Minimum Azimuth	0.965
Ellipsoid Minor	0.779
Bounds Y	0.639

3.2.1.3. Skewness and Kurtosis:

Some features have high skewness and kurtosis values, which might indicate that the distributions aren't normal or that there are outliers:

Feature	Skew	Kurtosis
Intensity Minimum	-2.60	5.28
Bound X	3.82	35.97
Centroid X	1.99	9.22

3.2.1.4. Bonferroni results

To control the increased risk of type I error associated with multiple comparisons in ANOVA, the Bonferroni correction method was applied.

The results of ANOVA before and after the Bonferroni correction are presented in Tables 3.1 and the table in the Appendix, respectively. Features with adjusted p-values below 0.05 were considered statistically significant.

Among all the characteristics that were compared, Volume, Minimum Intensity, and Centroid Z, provided statistically significant differences between seeding groups after Bonferroni correction. Specifically:

- Alginate was much greater in volume than Collagen ($p < 0.05$).
- Minimum Intensity fluctuated between both Alginate vs Collagen and Alginate vs Media.
- Centroid Z showed no statistically significant difference in ANOVA

Feature	Comparison	Raw p-value	Corrected p-value	Significant (Bonferroni)
Volume [ÂµmÂ³]	Alginate vs Collagen	0	0	TRUE
Volume [ÂµmÂ³]	Alginate vs Media	0.0494	0.4446	FALSE
Volume [ÂµmÂ³]	Collagen vs Media	0.4455	1	FALSE
Intensity Minimum	Alginate vs Collagen	0	0	TRUE
Intensity Minimum	Alginate vs Media	0	0	TRUE
Intensity Minimum	Collagen vs Media	0	0	TRUE
Centroid Z [Âµm]	Alginate vs Collagen	0	0	TRUE
Centroid Z [Âµm]	Alginate vs Media	0	0	TRUE
Centroid Z [Âµm]	Collagen vs Media	0	0	TRUE

3.2.1.5. Conclusion of ANOVA Statistical Analysis:

Intensity and spatial features like Centroid Z and Bounds Z were most heterogeneous between the groups. These are likely to capture biological variability in cell activity or scaffold-cell interaction and may be useful inputs for machine learning classifiers.

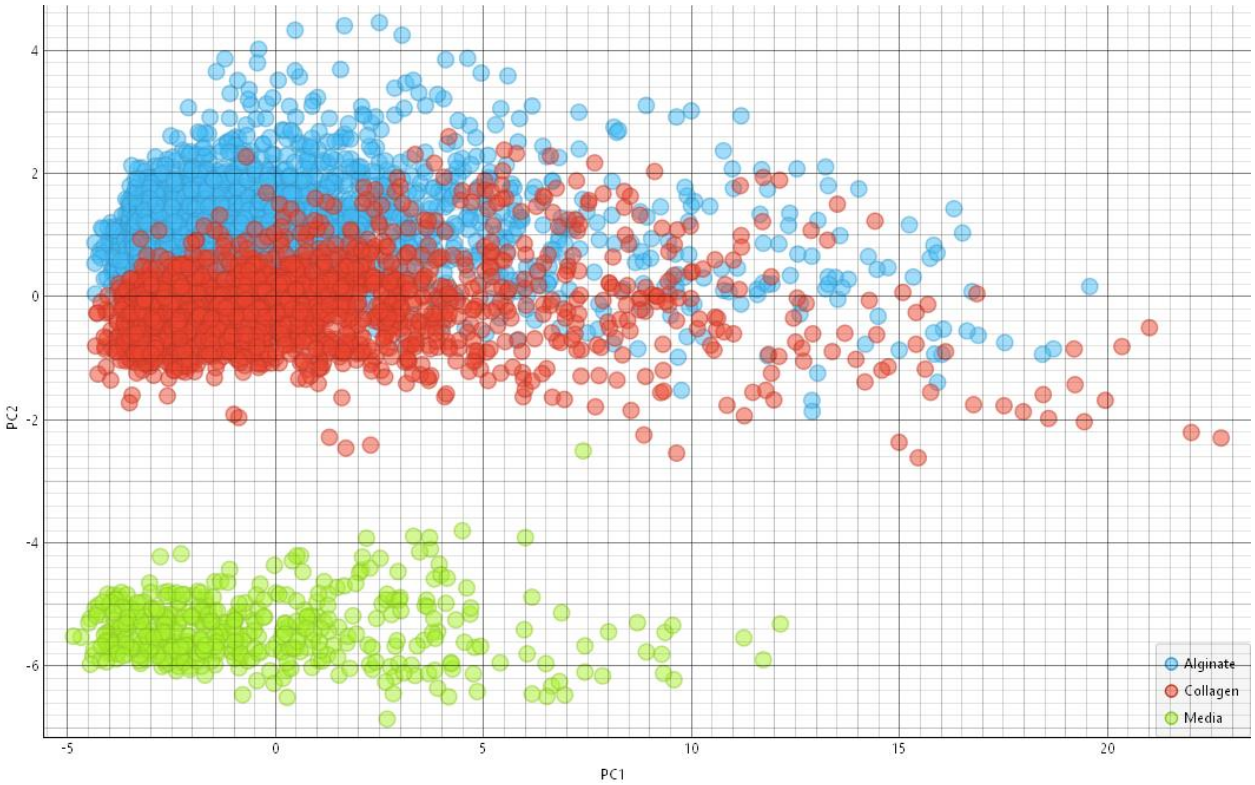


Figure 3.4. Principal Component Analysis (PCA) plot of discrimination between three cell-seeding conditions: Alginate (blue), Collagen (red), and Media (green), based on derived morphological and intensity-based features. PC1 (the x-axis) captures much of the variation, distinguishing Media from the rest of the data. PC2 (the y-axis) provides more discrimination. The lower-left quadrant clearly shows groups of media samples. Alginate and Collagen overlap slightly, showing that they have certain characteristics in common but also those that are different.

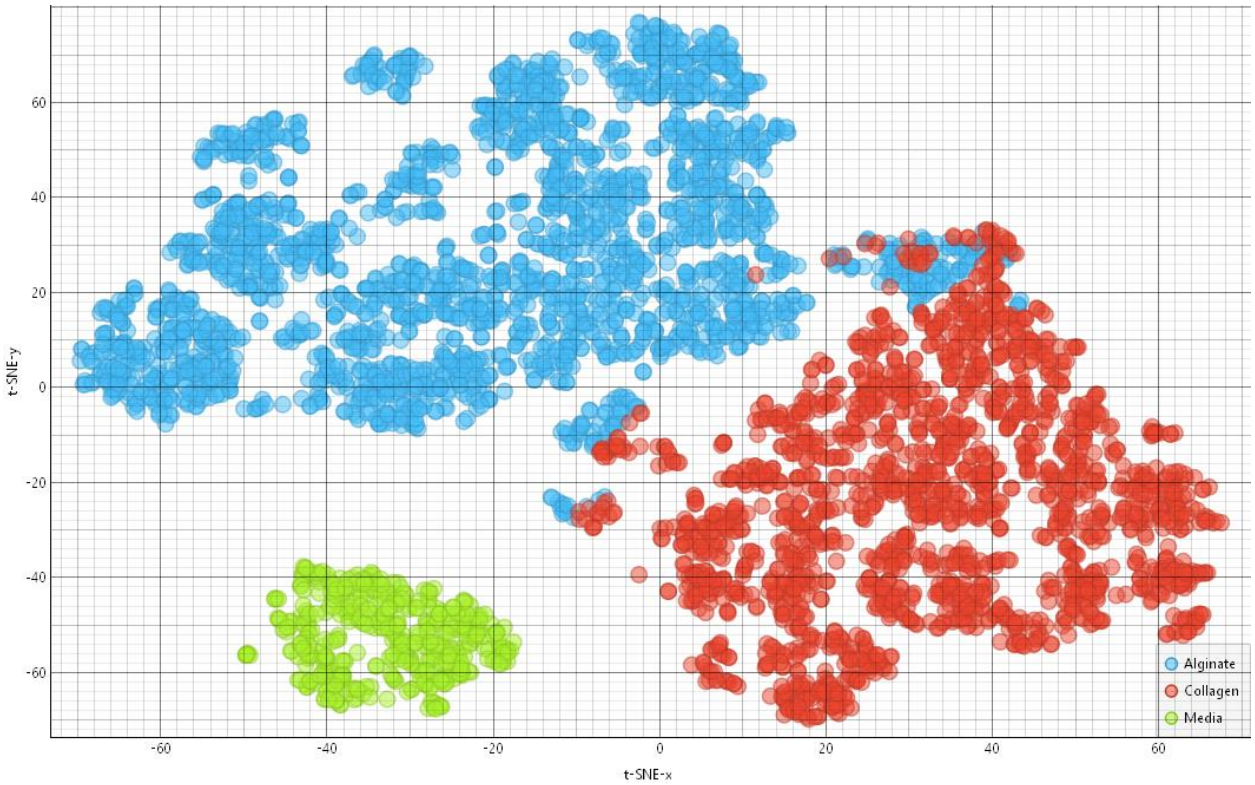


Figure 3.5. Two-dimensional t-SNE plot of the distribution of particles based on different cell seeding methods: Alginate (blue), Collagen (red), and Media (green). The nicely separated Media group from the others exhibits excellent distinctions in feature space. Although there is still some overlap, t-SNE reduces the data considerably better than PCA in separating the Alginate from the Collagen group. t-SNE has a better chance of revealing the underlying structure in the data due to its non-linear dimension reduction process.

3.3. Feature Engineering and Machine Learning

The aim in this step (Figure 3.4 and 3.5) was to prepare and leverage the most insightful attributes of data for training machine learning models which are capable of differentiating among the three methods of cell seeding including Alginate, Collagen, and Media, with good accuracy. Several key steps taken in this direction which might help to achieve this:

1. Feature Selection: Determining the most effective feature features for classification. Feature importance of Random Forest model and SHAP values helped to enable this.

2. Dimensionality Reduction: Employing techniques such as PCA and t-SNE helps reduce the number of features as well as easier class separation detection.

3. Feature Construction (if needed): Building new features by combining or re-transformation in order to improve model performance.

4. Model Building: Training multiple machine learning models, i.e., Random Forest, XGBoost, SVM, or KNN, to identify the best method of seeding the data.

5. Model Evaluation: Choosing the best model based on their accuracy performance, F1-score, precision, re-call, and AUC.

6. Explanation of the Model: By using explainable AI methods like SHAP and LIME to study how the model reaches its decision, we could make logical inferences about how it predicts the future.

The Figure 3.6 shows a decision tree for cell classification into three classes (Alginate, Collagen, and Media) based on intensity-related features.

The Intensity Minimum was used as the root node since it possessed strong group discrimination ability. Intensity Mean was also used in the second split with significant impact on model accuracy. This decision tree produced almost flawless classification accuracy, effectively distinguishing each group with exceptional precision.

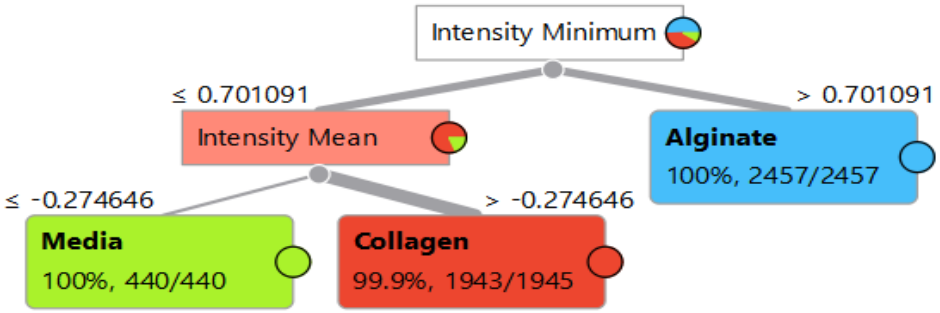


Figure 3.6. Decision tree model for cell classification based on intensity features.

In this process, the RANK tool of the Orange software was applied in order to identify the most significant features for cell classification [Figure 3.7]. Information Gain Ratio and Gini Index were used as two scoring methods to evaluate feature significance. The results revealed that Intensity Minimum and Intensity Mean were the most significant features accounting for discrimination among the three groups. Other features such as Centroid Z, Centroid Y, and Diameter were of lesser significance.

		#	Gain ratio	Gini
1	Intensity Minimum		0.525	0.441
2	Intensity Mean		0.209	0.137
3	Centroid Z [µm]		0.096	0.104
4	Intensity Maximum		0.096	0.052
5	Centroid Y [µm]		0.034	0.029
6	Intensity Standard Deviation		0.008	0.004
7	Feret Minimum [µm]		0.006	0.006
8	Diameter [µm]		0.006	0.007
9	Feret Ratio		0.004	0.003
10	Sphericity		0.003	0.003

Figure 3.7. Feature ranking based on Information Gain Ratio and Gini Decrease in the classification model.

In order to assess the separability of the chosen features, a Scatter Plot was plotted based on the two highest ranked features: Intensity Minimum and Intensity Mean [Figure 3.8]. As observed from the Figure 3.8, the three clusters (Alginate, Collagen, and Media), are extremely separable. This extreme separability signifies the excellent discriminatory power of these two features in distinguishing various cell seeding techniques on PLA scaffolds.

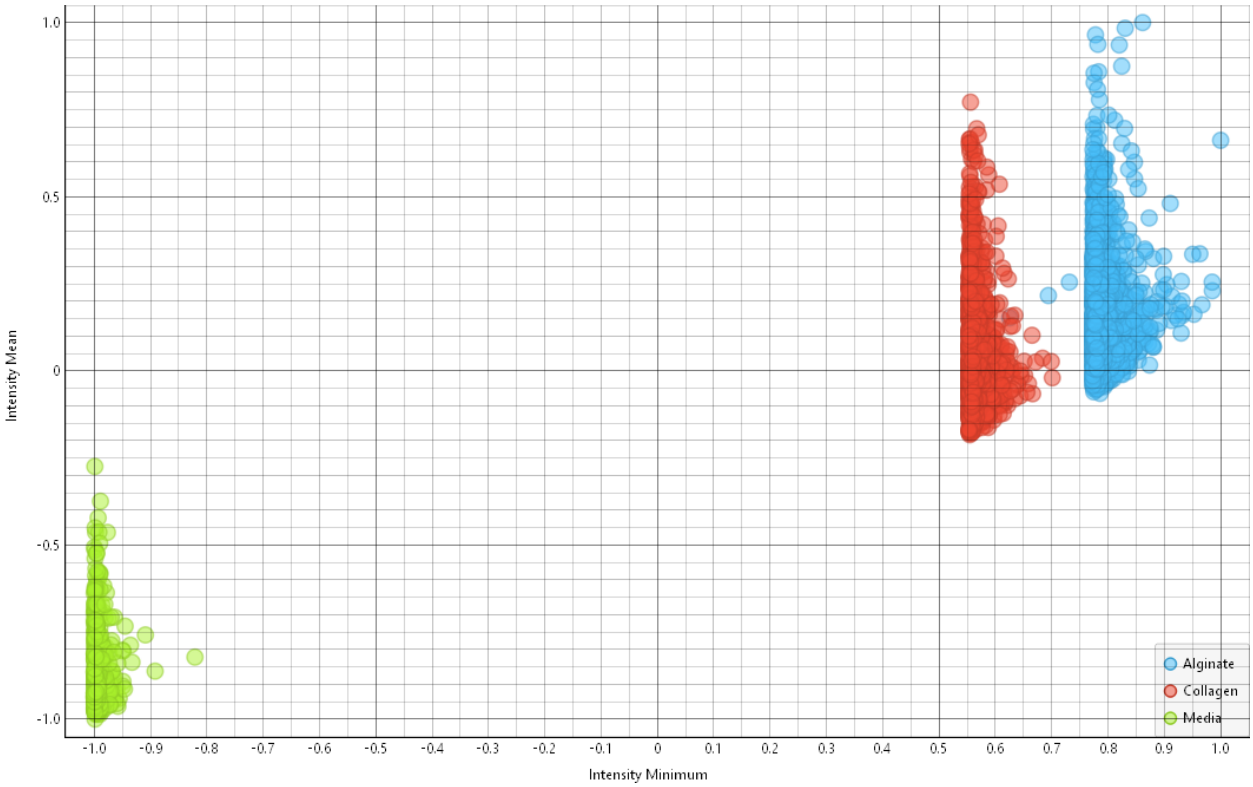


Figure 3.8. Scatter plot based on Intensity Minimum and Intensity Mean showing separability of the three cell groups.

To compare and assess the performances of different machine learning models, an initial analysis was conducted using Orange's Test and Score widget with 10-fold cross-validation on the entire data, as illustrated in Figure 3.9. Random Forest, SVM, and k-NN models were tried and tested with some performance measures like AUC, Classification Accuracy (CA), F1-score, Precision, Recall, and Matthews Correlation Coefficient (MCC).

Among the models tried, Random Forest initially came with the best performance, with AUC of 1.0 and classification accuracy well over 99.9%. With the entire dataset used in cross-validation, these performance values very likely indicate overfitting. To avoid this limitation and to guarantee model performance would extrapolate to test data, a more stringent three-way split of the data (60% training, 20% validation, 20% test) was later employed in Python. The final model was re-trained and tested on the held-out test set and achieved an AUC of 0.9999 and accuracy of 99.79%, thereby justifying the high predictive ability of the model with the avoidance of overfitting.

Model	AUC	CA	F1	Precision	Recall	MCC
Random Forest	1.000	0.999	0.999	0.999	0.999	0.998
SVM	1.000	0.986	0.986	0.986	0.986	0.975
kNN	0.992	0.961	0.961	0.961	0.961	0.931

Figure 3.9. Initial evaluation and comparison of machine learning models using 10-fold cross-validation on the entire dataset in Orange software. The high AUC values observed (e.g., AUC = 1.0 for Random Forest and SVM) may reflect overfitting, which was later addressed through separate test set validation in Python..

For classifying performance assessment, an ROC (Receiver Operating Characteristic) curve was plotted for each of the three classes: Alginate, Collagen, and Media [Figure 3.10]. The ROC curve indicates how the True Positive Rate is related to the False Positive Rate for each class.

The Random Forest model generated curves very close to the top-left region of the plot for each of the classes with excellent sensitivity and overall classification. The Area Under the Curve (AUC) for each of the classes was found to be 1.00, demonstrating the perfect ability of the model to distinguish among the groups.

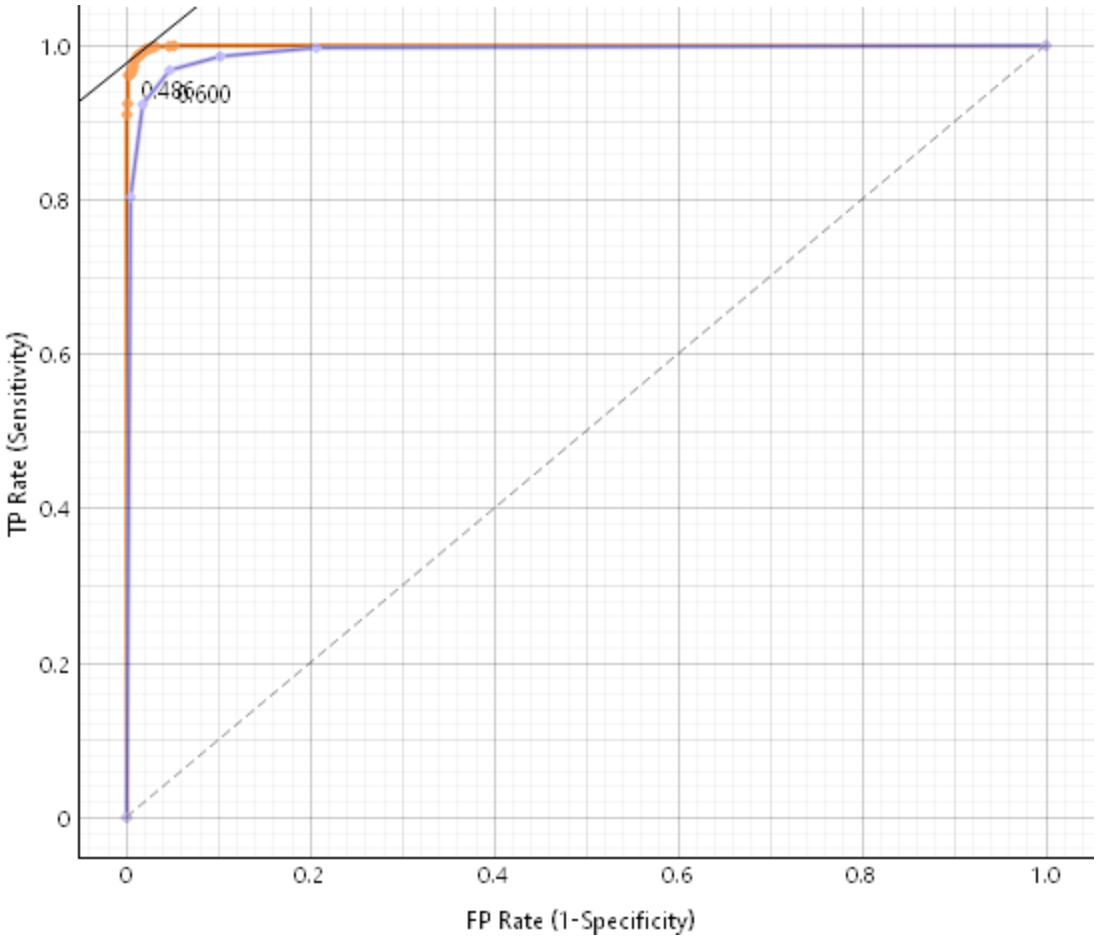


Figure 3.10. ROC curves of the Random Forest model for the three cell-seeding classes.

The generation of a Confusion Matrix, showing the number of true and false predictions for the Media, Collagen, and Alginate classes, allowed for a better measurement of the model's performance [Figure 3.11].

Random Forest model was highly precise with an error rate of less than 0.1% and only 3 misclassified samples out of 3390. Above all, the Media group was identified 100% accurately, and this also contributed to the improved performance of the model.

Data Table Mon Mar 03 25, 13:56:55

Data instances: 3390
Features: 10
Meta attributes: 13
Target: Class 'Class'

	Class	Random Forest (1)	SVM	kNN (1)	Random Forest (1) (Alginate)	Random Forest (1) (Collagen)	Random Forest (1) (Media)	SVM (Alginate)	SVM (Collagen)	SVM (Media)	kNN (1) (Alginate)	kNN (1) (Collagen)	kNN (1) (Media)	Fold	Feret Minimum [µm]	C [µ
1	Alginate	Alginate	Alginate	Alginate	0.98	0.02	0	0.871828	0.127514	0.000657901	1	0	0	1	-0.886911	(
2	Collagen	Collagen	Collagen	Collagen	0.01	0.99	0	4.74699e-07	0.999655	0.000345013	0	1	0	1	-0.547818	
3	Media	Media	Media	Media	0	0	1	6.31712e-07	7.58322e-07	0.999999	0	0	1	1	-0.659337	
4	Media	Media	Media	Media	0	0.0418182	0.958182	2.62943e-06	3.15703e-06	0.999994	0	0	1	1	-0.153839	
5	Collagen	Collagen	Collagen	Collagen	0	1	0	8.0186e-07	0.999551	0.000448502	0.4	0.6	0	1	-0.334642	
6	Collagen	Collagen	Collagen	Collagen	0	1	0	0.00189082	0.997605	0.000504555	0.2	0.8	0	1	0.325742	
7	Collagen	Collagen	Collagen	Collagen	0	0.994286	0.00571429	2.57782e-06	0.999192	0.000805125	0.2	0.8	0	1	-0.773909	
8	Alginate	Alginate	Alginate	Alginate	0.984286	0.0157143	0	0.804605	0.194873	0.00052209	0.6	0.4	0	1	-0.66082	
9	Collagen	Collagen	Collagen	Collagen	0	1	0	6.26135e-07	0.999603	0.000396312	0.2	0.8	0	1	-0.525305	
10	Collagen	Collagen	Collagen	Collagen	0	1	0	1.33562e-07	0.999817	0.000182921	0.2	0.8	0	1	-0.713351	
11	Collagen	Collagen	Collagen	Collagen	0	1	0	0.0103532	0.987835	0.00181173	0.2	0.8	0	1	-0.305585	
12	Collagen	Collagen	Collagen	Collagen	0	1	0	1.8243e-06	0.999321	0.000676926	0	1	0	1	-0.455846	
13	Collagen	Collagen	Collagen	Collagen	0	1	0	2.97172e-07	0.999727	0.000272915	0	1	0	1	-0.773909	
14	Alginate	Alginate	Alginate	Alginate	1	0	0	0.999111	0.000728051	0.000160552	1	0	0	1	-0.66082	
15	Alginate	Alginate	Alginate	Alginate	1	0	0	0.997868	0.00179238	0.000339348	1	0	0	1	-0.66082	
16	Collagen	Collagen	Collagen	Collagen	0	1	0	9.85311e-07	0.999502	0.000497475	0	1	0	1	-0.886911	
17	Alginate	Alginate	Alginate	Alginate	1	0	0	0.999678	3.76333e-06	0.000318013	1	0	0	1	-0.773909	
18	Alginate	Alginate	Alginate	Alginate	1	0	0	0.778461	0.220236	0.00130255	0.6	0.4	0	1	-0.576789	
19	Alginate	Alginate	Alginate	Alginate	1	0	0	0.96847	0.0312792	0.000250661	0.8	0.2	0	1	-0.774258	(
20	Collagen	Collagen	Collagen	Collagen	0	1	0	0.002717	0.996698	0.000584784	0	1	0	1	-0.105934	
21	Collagen	Collagen	Collagen	Collagen	0	1	0	2.78991e-06	0.999159	0.00083785	0	1	0	1	-0.152531	
22	Media	Media	Media	Media	0	0	1	2.89741e-06	3.47996e-06	0.999994	0	0	1	1	-0.773909	
23	Alginate	Alginate	Alginate	Alginate	1	0	0	0.99926	0.000428656	0.000311216	1	0	0	1	-0.809686	
24	Alginate	Alginate	Alginate	Alginate	0.992	0.008	0	0.966498	0.033229	0.000272826	1	0	0	1	-0.719808	
25	Collagen	Collagen	Collagen	Collagen	0.0128571	0.956104	0.031039	4.85124e-06	0.999002	0.000993245	0.4	0.6	0	1	-0.576789	
26	Alginate	Alginate	Alginate	Alginate	1	0	0	0.998612	0.0011093	0.000278222	1	0	0	1	-0.809686	
27	Alginate	Alginate	Alginate	Alginate	1	0	0	0.998039	0.00163129	0.00032923	0.8	0.2	0	1	-0.714223	
28	Collagen	Collagen	Collagen	Collagen	0	1	0	1.09257e-06	0.999475	0.000523416	0	1	0	1	-0.809686	
29	Collagen	Collagen	Collagen	Collagen	0	1	0	2.51022e-06	0.999455	0.000542103	0.4	0.6	0	1	-0.321728	
30	Collagen	Collagen	Collagen	Collagen	0	1	0	3.57274e-07	0.9997	0.000299462	0	1	0	1	-0.66082	
31	Collagen	Collagen	Collagen	Collagen	0	0.976667	0.0233333	0.0020237	0.995955	0.00202169	0.2	0.8	0	1	-0.095637	
32	Collagen	Collagen	Collagen	Collagen	0	1	0	9.97957e-07	0.999502	0.000496544	0	1	0	1	-0.505585	
33	Alginate	Alginate	Alginate	Alginate	1	0	0	0.9987	0.000970117	0.000330095	1	0	0	1	-0.886911	
34	Alginate	Alginate	Alginate	Alginate	1	0	0	0.989638	0.00999904	0.000362875	1	0	0	1	-0.773909	
35	Alginate	Alginate	Alginate	Alginate	1	0	0	0.998446	0.00112549	0.000428443	0.6	0.4	0	1	-0.607504	
36	Collagen	Collagen	Collagen	Collagen	0.0225165	0.977484	0	2.07119e-06	0.999448	0.00055015	0.2	0.8	0	1	-0.793281	
37	Alginate	Alginate	Alginate	Alginate	1	0	0	0.99977	6.28475e-05	0.000167315	1	0	0	1	-0.798168	(
38	Collagen	Collagen	Collagen	Collagen	0	1	0	7.74759e-07	0.999563	0.000436154	0	1	0	1	-0.773909	
39	Alginate	Alginate	Alginate	Alginate	0.98	0.0133333	0.00666667	0.997347	0.00242876	0.00022426	1	0	0	1	-0.321728	-(
40	Media	Media	Media	Media	0	0.04	0.96	4.51365e-06	5.42022e-06	0.99999	0	0	1	1	-0.18377	
41	Alginate	Alginate	Alginate	Alginate	1	0	0	0.997371	0.00236169	0.000267406	1	0	0	1	-0.321728	(
42	Collagen	Collagen	Collagen	Collagen	0	1	0	3.4641e-07	0.999705	0.000294744	0	1	0	1	-0.773909	
43	Media	Media	Media	Media	0	0	1	0.002588	0.00588807	0.991524	0	0	1	1	-0.708552	
44	Collagen	Collagen	Collagen	Collagen	0	1	0	6.10222e-07	0.999608	0.000391458	0	1	0	1	-0.556981	
45	Alginate	Alginate	Alginate	Alginate	1	0	0	0.997951	0.0017618	0.000286971	0.8	0.2	0	1	-0.415445	
46	Alginate	Alginate	Alginate	Alginate	1	0	0	0.978125	0.0215701	0.000304431	1	0	0	1	-0.369285	0.
47	Alginate	Alginate	Alginate	Alginate	1	0	0	0.995928	0.00375522	0.000317208	1	0	0	1	-0.701745	
48	Alginate	Alginate	Alginate	Alginate	1	0	0	0.991735	0.00759164	0.000673707	1	0	0	1	-0.773909	(
49	Alginate	Alginate	Alginate	Alginate	1	0	0	0.99748	0.00221258	0.00030723	0.8	0.2	0	1	-0.321728	
50	Alginate	Alginate	Alginate	Alginate	1	0	0	0.825612	0.174077	0.000311553	1	0	0	1	-0.580017	
51	Collagen	Collagen	Collagen	Collagen	0	1	0	3.09514e-07	0.999741	0.000258785	0	1	0	1	-0.651309	
52	Media	Media	Media	Media	0	0.02	0.98	0.000791704	0.00173275	0.997476	0	0	1	1	-0.773909	
53	Alginate	Alginate	Alginate	Alginate	1	0	0	0.997953	0.00186651	0.000180833	1	0	0	1	-0.405323	(
54	Collagen	Collagen	Collagen	Collagen	0	1	0	8.75936e-07	0.99953	0.000469011	0	1	0	1	-0.247993	
55	Collagen	Collagen	Collagen	Collagen	0	1	0	5.60391e-07	0.99963	0.000369098	0	1	0	1	-0.39363	(
56	Collagen	Collagen	Collagen	Collagen	0.0345	0.9655	0	9.76808e-07	0.999504	0.000495184	0.2	0.8	0	1	-0.759162	
57	Alginate	Alginate	Alginate	Alginate	1	0	0	0.999474	0.000307146	0.000219207	0.8	0.2	0	1	-0.658028	
58	Collagen	Collagen	Collagen	Collagen	0	1	0	1.64755e-07	0.999797	0.000203106	0	1	0	1	-0.684031	
59	Collagen	Collagen	Collagen	Collagen	0	1	0	4.22011e-07	0.999674	0.000325493	0	1	0	1	-0.372775	
60	Collagen	Collagen	Collagen	Collagen	0	1	0	3.46241e-07	0.999705	0.000294598	0	1	0	1	-0.47356	
61	Collagen	Collagen	Collagen	Collagen	0	1	0	1.22464e-06	0.999453	0.000546202	0	1	0	1	-0.886911	
62	Alginate	Alginate	Alginate	Alginate	1	0	0	0.998809	0.000856977	0.000334521	1	0	0	1	-0.525305	(
63	Collagen	Collagen	Collagen	Collagen	0	1	0	9.30198e-07	0.999516	0.00048311	0	1	0	1	-0.686562	
64	Collagen	Collagen	Collagen	Collagen	0	1	0	4.63681e-07	0.999658	0.00034138	0	1	0	1	-0.66082	
65	Collagen	Collagen	Collagen	Collagen	0	0.984667	0.0153333	0.00705704	0.991505	0.00143756	0	1	0	1	-0.409599	
66	Alginate	Alginate	Alginate	Alginate	0.981111	0.0188889	0	0.991925	0.00771865	0.000356022	0.8	0.2	0	1	-0.455061	
67	Alginate	Alginate	Alginate	Alginate	1	0	0	0.953635	0.0460752	0.000289338	1	0	0	1	-0.736824	
68	Alginate	Alginate	Alginate	Collagen	1	0	0	0.937385	0.0618624	0.00075241	0.4	0.6	0	1	-0.354712	
69	Collagen	Collagen	Collagen	Collagen	0	1	0	3.73051e-07	0.999694	0.000305816	0	1	0	1	-0.773909	
70	Alginate	Alginate	Alginate	Alginate	1	0	0	0.999566	0.000149939	0.000284496	1	0	0	1	-0.773909	0.

Figure 3.11. Confusion matrix of the Random Forest model showing prediction accuracy for each class.

3.4. Final Model Assessment

After training and validation on 80% data with 10-fold cross-validation on the Random Forest classifier, the model was evaluated on the 20% held-out test set. The model was 99.79% accurate, 99.69% macro-averaged F1-score, and multi-class AUC of 0.9999. The model was 99.79% accurate, 99.69% macro-averaged F1-score, and 0.9999 multi-class AUC. Confusion matrix brought about the fact that the model mis-predicted only two samples among 969 test examples, which reflects good model generalization.

Thus, the above results confirm the reproducibility of the imaging features extracted and the Random Forest approach in separating the different seeding techniques.

Metric	Value
Accuracy	99.79%
F1-score (macro)	99.69%
AUC (multi-class)	0.9999
Misclassified samples	2 out of 969

3.5. Model Interpretation and Explainability

At this stage, the goal was to move beyond treating the machine learning model, particularly the Random Forest, as a "black box." Instead, explain-ability tools were used to better understand which features most influenced the model's decisions.

Two main techniques were applied which can be seen in Figure 3.12.

3.5.1. Feature Importance

Using the embedded feature importance scores of the Random Forest model, the most relevant features were determined based on how frequently they were used for splitting decisions in the trees. The key features included Intensity Minimum, Intensity Mean, Centroid Z, and Intensity Maximum.

These results showed that the intensity characteristics and the spatial information (more specifically the Z-coordinate) played an important role in the splitting of the seeding groups.

3.5.2. SHAP (SHapley Additive Explanations)

To obtain a more precise and individualized interpretation of model behavior, SHAP values were calculated. These are the extents to which each feature value drove the ultimate prediction for all samples. The SHAP summary plot indicated that Intensity

Minimum contributed the most positively towards classifying samples of the Media group. further, Centroid Z and Intensity Mean also contributed significantly but moderately. finally, this analysis confirmed the model's explanation and facilitated trusting its predictions.

3.5.3. Conclusion of Model Interpretation and Explain-ability:

The SHAP and Feature Importance analysis together recognized intensity-based and spatial features as the leading contributors to the classification accuracy. This interpretability step adds to the scientific validity of the model and encourages its application in tissue engineering research.

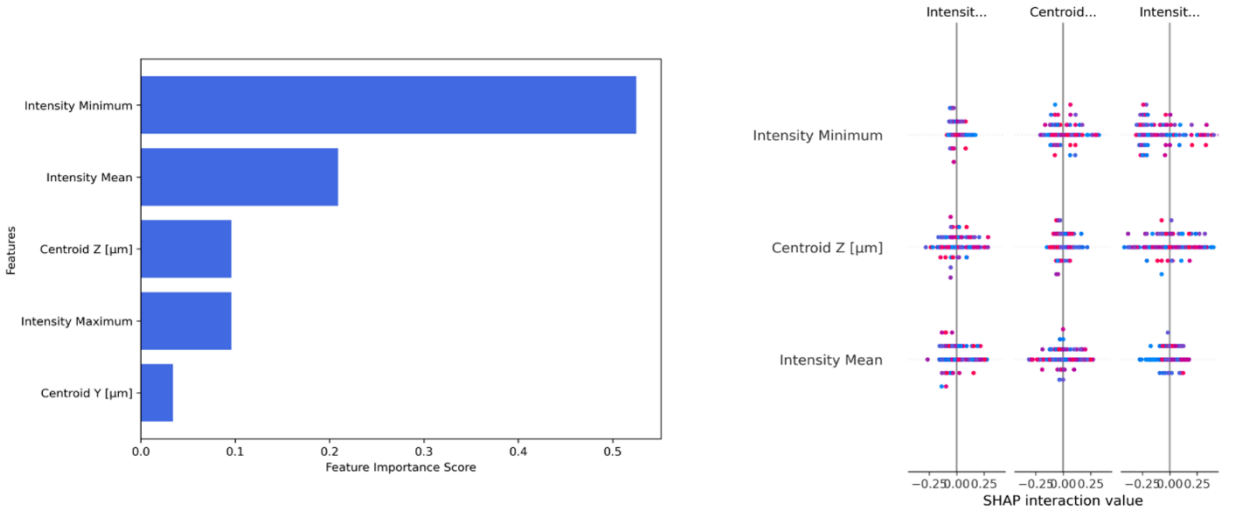


Figure 3.12 Comparison of feature importance in the Random Forest model (left) and SHAP interaction values (right). The left plot finds significant predictive attributes, i.e., Intensity Minimum and Intensity Mean, as most crucial in determining the classification. The SHAP interaction plot (right) highlights how features interact with one another to affect the predictions of the model, increasing the interpretability of the classifier.

3.6. Summary of Results

This study aimed to classify biomaterial scaffolds based on particle-level characteristics extracted from imaging data. Using a combination of statistical analysis and machine learning models, the most informative features were identified through methods such as Random Forest feature importance and SHAP analysis.

The findings showed that the three most influential variables in the prediction of the scaffold class were Intensity Minimum, Intensity Mean, and Centroid Z [µm].

The best machine learning model that was examined in the current study was the Random Forest classifier, which had an accuracy of approximately 90%. In addition, the current study findings show that it is possible to classify and evaluate biomaterial scaffolds in tissue engineering applications successfully using the combination of image-based quantitative data and machine learning.

4.Discussion

This study demonstrates that the cell seeding strategy exerts a profound influence on cell distribution, morphology, and viability within 3D-printed PLA scaffolds mimicking trabecular bone. By comparing suspension (media-only) seeding to hydrogel-based seeding (cells delivered in 2% alginate or 0.5% collagen), we observed distinct patterns in the quantitative imaging features. The Random Forest model also found that the lowest and mean intensity of fluorescence and the centroid Z spatial location were the most efficient ways for distinguishing groups from each other. In addition, SHAP analysis showed that media-suspension group classification was strongly affected by a higher minimum intensity. This implies that the background fluorescence of the cells plated on normal media was always brighter with fewer very dark regions compared to the cells encapsulated in hydrogels. Biologically, this may mean that suspension-seeded cells were more homogeneously stained or had fewer dead/dim cells, whereas hydrogel-seeded cells had a wider intensity range. This may be attributed to light scattering or the presence of low-intensity regions within the gel matrix. Similarly, Centroid Z was a characteristic feature which indicated a difference in the cell penetration depth of the two approaches. Suspension seeding would most likely have resulted in the majority of the cells remaining at the scaffold surface. However, cell encapsulation in alginate or collagen enabled them to be positioned deeper into the pores. Indeed, we found that the hydrogel-based groups achieved a more homogeneous cell distribution throughout the scaffold's thickness, whereas the suspension group's cells were concentrated more superficially. These quantitative insights are in line with expectations; a more uniform spatial distribution is crucial for effective tissue formation in large scaffolds, and our data indicate the seeding method is a determining factor.

The morphological descriptors (e.g. Feret diameters, ellipsoid aspect ratios) further underscored how cell shape and clustering differed by seeding strategy (Figure 3.1 and 3.2). Cells delivered in collagen showed a tendency toward elongated or spread morphologies (greater differences between Feret max and min diameters), whereas those in alginate remained more rounded, consistent with the nature of these matrices. Collagen provides a biomimetic extracellular matrix environment that can support cell adhesion and spreading, while alginate (without RGD or other cell-binding motifs) tends to keep cells rounded within its gel.[41] Our observations align with Glowacki et al. findings that collagen-

based scaffolds inherently promote cell attachment and growth since collagen has regions to which cells bind.[35] Alginate, on the other hand, is called a bioinert hydrogel – highly biocompatible and easily gelating, but having no integrin-binding regions.[42] Cells encapsulated in pure alginate are rounded and less spread, and this might explain the smaller Feret diameters and high circularity we observed for that group. The alginate group, on the other hand, showed a more even distribution of cells throughout the scaffold. This suggests that the cells were kept in spherical shape and were evenly spread out. This finding is significant because it shows that one can achieve even cell dispersion with alginate entrapment, albeit potentially at the expense of cell-matrix interactions that facilitate spreading. Researchers have acknowledged this trade-off and investigated changes to alginate (e.g., grafting RGD peptides or mixing with ECM proteins) to enhance cell adhesion and functionality.[41,42] For instance, Neves et al. (2020) demonstrated that tuning alginate's composition and stiffness can markedly enhance its performance as a 3D cell microenvironment.[41,42] In our case, even using unmodified alginate, we achieved good initial cell viability and distribution, but one might expect even better cellular behavior (such as migration or differentiation) if alginate were biofunctionalized in future studies.

When comparing directly to previous literature, our results fit well with known challenges and solutions in scaffold-based tissue engineering. It is well documented that seeding cells into pre-made porous scaffolds using static (gravity-driven) methods often results in incomplete and uneven cell distribution. Chan and Leong (2008) note that post-fabrication cell seeding has "limited penetration ability" and typically leads to an inhomogeneous cell pattern inside.[68] In our suspension-seeded samples, we indeed observed evidence of this phenomenon, with cells mostly on outer regions and fewer deep inside, which might be a problematic outcome also highlighted by other researchers as it can cause the interior of a scaffold to be cell-poor or even necrotic during culture.[68] Various strategies like agitation or perfusion can improve seeding efficiency, but these come with issues such as increased cell shear stress, lower viability, and higher complexity.[68] By contrast, encapsulating cells within a hydrogel carrier before introducing them into the scaffold can circumvent many of these issues. This method essentially turns seeding into a one-step embedding process: cells are mixed with a liquid biomaterial (alginate or collagen solution) which is then gelled in situ, achieving a much more uniform initial distribution.

As the same review emphasizes, this approach yields homogeneous cell distribution throughout the scaffold and excellent cell viability, owing to the gentle, conformal encapsulation of cells.[68,69] Our findings strongly support this: both alginate and collagen cell-seeded scaffolds had cells present in nearly all regions of the porous network from the start, something the suspension method could not accomplish. Cell retention in the scaffold was also visibly higher in the hydrogel groups, because the hydrogels likely prevented cells from simply washing out of the pores, a common problem in static seeding. Importantly, we did not observe major cell aggregation at the seeding stage in the hydrogel groups, which means the cells were fairly individually encapsulated and well-dispersed (consistent with the “homogenous cell distribution” reported for hydrogel seeding.[68] This even seeding is critical for subsequent tissue development, as a uniform cell population can lead to more uniform extracellular matrix deposition and mineralization over time, which is desirable for regenerating functional bone tissue. Our work thus provides empirical evidence reinforcing the consensus in tissue engineering; simply seeding cells by pipetting onto scaffolds is inadequate for large 3D constructs, and the use of a carrier (like a hydrogel) markedly improves the initial cell layout.[68]

Between the two hydrogel strategies we examined, the collagen-based seeding emerged as particularly effective. Both methods (alginate and collagen) achieved good distribution, but qualitative and quantitative indications suggest that the collagen group might confer additional advantages. Collagen, being a natural component of bone ECM, not only distributed cells evenly but also provided them with an environment conducive to attachment. After seeding and subsequent culture, cells in collagen showed more evidence of spreading and forming cell–cell connections (consistent with the elongated shapes captured by our imaging), whereas alginate-encapsulated cells largely remained isolated and round. This difference is in line with Kim et al. (2011), who designed a coaxial scaffold combining collagen and alginate to capitalize on the strengths of both: collagen’s cell-favorable interface and alginate’s mechanical support and mild gelation.[36] In their work, a collagen shell promoted cell attachment and skin regeneration, while an alginate core provided structural integrity.[36] In our context, the collagen hydrogel itself performed well as the cell carrier within a strong PLA scaffold, essentially acting as a bioactive filler in the pores. The outcome was a hybrid scaffold with the robust architecture of PLA and

the bioactivity of collagen, which appears to support cell colonization more effectively than the purely synthetic scenario. This approach of hybridizing synthetic scaffolds with natural hydrogels has been reported in prior studies. For example, Markovic et al. (2015) embedded cells in a photocrosslinkable gelatin (a derivative of collagen) within 3D printed scaffolds and observed uniformly distributed cells and high seeding efficiency.[19] Our results agree with the results of Markovic study; the collagen-containing method (analogous to gelatin in their case) clearly facilitated better initial cell seeding. We also note that cell viability in the collagen group was very high post-seeding – likely attributable to collagen's excellent biocompatibility and the gentle neutralization/polymerization process of the collagen gel. Alginate also maintained good viability (we did not detect significant cell death immediately after seeding in either hydrogel condition), but in the longer term, cells in alginate might experience a less favorable environment unless the alginate is progressively degraded or modified to allow cell spreading. Nonetheless, from a tissue engineering perspective, both hydrogel strategies have merit: alginate offers simplicity and uniformity, while collagen offers bio-functionality. The choice may depend on the specific application – e.g., alginate might be preferred for short-term cell delivery or when one wants a temporary cell carrier that eventually dissolves, whereas collagen may be better for applications needing cell-matrix interaction for differentiation (such as osteogenic maturation in bone scaffolds). In any case, our data strongly support the use of some form of matrix-assisted seeding for populating porous scaffolds, as opposed to direct cell suspension alone.

An interesting implication of the centroid Z feature being important is the role of scaffold geometry and gravity in cell placement. The PLA scaffolds used in the current study, mimics trabecular bone, with high porosity and interconnected pores. Even so, when cells were added in suspension, their initial settling was biased toward upper layers (closer to where the droplet was applied), resulting in a non-uniform depth distribution. In a living system or in dynamic culture, cells can migrate or be convected deeper over time, but initial placement is critical. The alginate and collagen methods, by contrast, effectively "pre-positioned" cells throughout the full depth during gel infusion. This resulted in significantly higher scaffold colonization – i.e., a greater fraction of the scaffold volume containing cells – right from the start. Achieving uniform cell colonization in bone graft

scaffolds is vital for successful regeneration, as it ensures that all regions of the graft receive cellular activity (matrix deposition, remodeling, and, eventually, mineralization).[68] If large portions of the interior remain acellular, they can become necrotic or fail to integrate with host tissue. Thus, our finding that the collagen seeding method produces the best colonization is particularly promising for bone tissue engineering. We speculate that a collagen-based seeding not only places cells uniformly but may also promote their migration and proliferation in subsequent culture. Collagen is a natural substrate that cells can enzymatically re-model; thus cells in collagen might slowly spread beyond their initial location, further improving distribution over time. Alginate, unless modified or partially oxidized, is not degradable by mammalian cells, so encapsulated cells tend to stay where they are. Future modifications to the alginate (e.g. making it partially degradable or adding adhesion peptides) could allow cells to migrate out and interact with the PLA scaffold surface more freely, potentially combining uniform seeding with long-term connectivity.

The use of Leica THUNDER imaging and machine learning analysis in this study also deserves discussion, as it represents an innovative approach to quantitatively evaluate seeding outcomes. The THUNDER microscope enabled high-resolution, optically sectioned images of cells deep inside the opaque PLA scaffold. Conventional microscopes often struggle with imaging within thick, scattering scaffolds, but the THUNDER's computational clearing allowed us to visualize and measure cell morphology throughout the 3D structure. This advanced imaging was essential for extracting reliable quantitative features (intensity, shape, location) from all cell "particles" in the scaffold, providing the rich dataset needed for machine learning. By applying a Random Forest classifier to these features, we could classify between the seeding methods objectively with nearly 90% accuracy. That kind of classification accuracy points out that the differences produced by each seeding method are consistent and sharp, essentially, the model could look at the patterns in the cell features and tell which method had been used. Such a result provides confidence in our experimental observations and also illustrates the power of machine learning in this context. Traditional statistical analysis might have identified one or two differing parameters between groups (e.g. "cells in collagen were significantly more elongated than in alginate"), but the ML approach considers the multivariate pattern. It essentially synthesizes a combination of features that together best

characterize each seeding condition. For instance, a suspension-seeded scaffold might be characterized by the model as “lower centroid Z + higher intensity minimum + moderate roundness,” whereas a collagen-seeded one might be “higher centroid Z + lower intensity min + higher aspect ratio,” etc. The Random Forest was particularly suitable here given its ability to handle non-linear feature interactions and its robustness with relatively small datasets. Our model’s strong performance suggests that such data-driven classification could be used as a tool in scaffold optimization; for example, to rapidly screen if a new seeding protocol yields distributions similar to an established optimal method.

Importantly, we leveraged explainable AI techniques (SHAP values and feature importance) to interpret the model’s decision-making, which adds scientific value beyond a black-box prediction. The SHAP analysis confirmed intensity minimum, intensity mean, and centroid Z were the peak contributors to the classification, which agrees with our outcomes that seeding strategies make differences. This agreement between the model’s “opinion” and human intuition builds trust in the model. For example, it would have been concerning if the model’s accuracy hinged on some obscure feature with no biological relevance; instead, it relied on features we can rationalize (brightness and spatial location of cells). The explain-ability plots also provided detailed insight. For instance, they indicated how varying a feature like intensity or cell size in one group affects the probability of classification into that group. This approach is still relatively novel in tissue engineering, but it can greatly aid in bridging the gap between data science and biology. As Jovel and Greiner (2021) explained, contemporary biomedical science is ever-more embracing machine learning methodologies, and interpretability tools guarantee these models are interpretable and can be relied upon by scientists.[43] 43 Our research is a prime example of this phenomenon in the field of tissue engineering. By interpreting the model, we essentially performed an computational analysis of what makes a “good” vs “poor” seeding: high overall cell fluorescence and deep penetration (features which the model linked to the hydrogel groups) can be considered signatures of a successful seeding protocol. This kind of insight is valuable because it quantitatively supports design decisions. For instance, one could use these features as target metrics when trying new seeding methods or scaffold materials. Statistical analysis confirmed that seeding

strategy significantly affects certain quantitative image features. Variation in Volume and Minimum Intensity shows that hydrogel-based methods (specifically, alginate) affect cell morphology and viability. Centroid Z, although not found to be statistically significant as identified by ANOVA, was an extremely high-ranked informative feature in the predictive models, which suggests its indicative significance in the spatial distribution analysis. This inter-disciplinary approach assures the practicality of combining classical statistics with predictive modeling.

In light of these findings, the implications for tissue engineering and scaffold design are clear. First, choosing an appropriate cell delivery method is just as crucial as scaffold material or architecture when the goal is to achieve uniform tissue formation. Even the most well-designed scaffold (optimal porosity, stiffness, biomaterial, etc.) will not fulfill its potential if cells are not effectively introduced throughout its volume.[68] Our results show that incorporating a hydrogel-based seeding step can dramatically improve initial cell distribution in a PLA bone scaffold. In reality, this means that bone graft tissue engineers or engineers of other thick tissue structures need to consider hybrid seeding strategies; e.g., seed the porous scaffolds with a cell-laden collagen or fibrin gel at seeding, or even co-print cells with bioinks into the scaffold structure. Both worlds are then utilized to their full potential; the scaffold provides mechanical integrity and 3D geometry definition, while the hydrogel provides a cell-friendly environment and even cell distribution. Indeed, the idea of hybrid scaffolds is gaining attractions; Kim et al. (2011) and Markovic et al. (2015) are leading instances of the combining of synthetic scaffolds with natural hydrogels towards better cell seeding and tissue outcomes.[19,36] The present study is further proof towards validating such approaches, especially in osteogenic scaffolds. For scaffolds mimicking trabecular bone (which inherently have a high surface area and complex pore network), a matrix-assisted seeding is likely indispensable to achieve the goal of uniform cell colonization (i.e., every pore hosting viable cells). Additionally, the success of the collagen method suggests that bioactivity matters; simply holding cells in place (as alginate does) is beneficial but providing a bioactive matrix (collagen) that cells can engage with yields even better early outcomes. Scaffold design should thus integrate not only mechanical considerations but also biological ones. For example, coating synthetic scaffold struts with collagen or other ECM proteins might replicate some benefits of the

collagen seeding method by encouraging cell attachment on scaffold surfaces. There is a trade-off to consider; adding hydrogels or coatings can impede mass transfer or alter mechanical properties. In our experiment, the thin hydrogels did not prevent perfusion of media through the scaffold (indeed, all groups were cultured with medium flow in a bioreactor), and the PLA provided mechanical stability so that the gels did not bear load. This suggests that an integrated design, where a sturdy scaffold is combined with a minimal amount of cell-laden matrix, can strike a balance between structural integrity and biological performance.

Finally, our use of machine learning for analysis highlights an emerging paradigm for scaffold development. Traditionally, evaluating a seeding method would require qualitative microscopy and perhaps manual counting of cells in different region, methods that are labor-intensive and subject to observer bias. Here, by training an algorithm on image-derived data, we achieved an objective, reproducible means of comparison. This approach can be extended beyond just assessing seeding techniques; for instance, machine learning models could be trained to predict longer-term outcomes (like the extent of mineralized tissue formed in a scaffold after a few weeks) based on early imaging features. Such predictive modeling is aligned with the broader trend of using AI to accelerate tissue engineering research.[44,49] Recent reviews underscore that machine learning can assist at many stages; from scaffold design optimization (e.g. predicting optimal pore size, material composition) to process control (e.g. real-time monitoring of bioprinting) and outcome prediction. Our results contribute to this narrative by showing that even in a relatively small-scale study, ML added value by distilling complex imaging data into actionable information. As a result, we not only determined that collagen seeding was best, but we also understand why in terms of quantifiable features. This synergy of advanced imaging and AI could be widely useful, for example, in comparing the impact of various scaffold shapes on cellular growth, or in comparing how cell types behave in the same scaffold. Through the use of such technologies, tissue engineers will better make informed decisions based on data, ultimately moving to faster invention of effective tissue-engineered scaffolds.[51]

Finally, the description of our findings shows that the 0.5% collagen seeding method provided the optimal results in terms of even cell distribution and scaffold infiltration,

followed by the alginate method, while the traditional suspension seeding was less effective. These differences, quantified via imaging features and confirmed by machine learning, mirror the insights from prior studies and reinforce key principles in scaffold-based tissue engineering; uniform initial cell seeding, and a cell-supportive microenvironment are pivotal for successful tissue development. Our use of a cutting-edge imaging platform (THUNDER) and interpretable machine learning not only allowed us to reach these conclusions with confidence but also represents an innovative model for studying and optimizing tissue engineering approaches. The combination of quantitative microscopy and machine learning analysis can be envisioned as a useful resource for the tissue engineer, enabling more clarity into the impact that design and methodological choices have on biological response. This approach, in conjunction with strategic integration of biomaterials (e.g., collagen) into scaffold systems, offers new opportunities for more effective and prophesying engineering of complex tissues such as bone.

5.Conclusion

In this project, we intended to determine how different cell seeding strategies influence cell behavior in a 3D printed bone-mimicking scaffold, and to identify which method yields the best outcome for tissue engineering applications. Using PLA scaffolds designed to replicate trabecular bone architecture, we compared a traditional suspension seeding (cells in culture medium) against two hydrogel-based seeding methods (cells mixed in 2% alginate or in 0.5% collagen). We then applied high-resolution fluorescence imaging (Leica THUNDER) to capture the resulting cell distributions and morphologies and leveraged machine learning (Random Forest classifier with SHAP explain-ability) to analyze the multi-parameter data. The findings of this comprehensive analysis can be summarized as follows:

- **Impact of seeding strategy on cell distribution and morphology**: The three methods produced quite dissimilar patterns of cell distribution throughout the scaffold. Suspension seeding led to cells piling up near the scaffold surface and the most irregular pattern of distribution. On the other hand, hydrogel-based approaches achieved far better cell dispersal, with the cells spread right throughout the depth of the scaffold. Incidentally, cells that were seeded into the collagen gel exhibited evidence of spreading and connected growth, whereas alginate-encapsulated cells were rounded in shape. These observations indicate that seeding within a supporting matrix (especially a bioactive one like collagen) allows for better and more biomimetic population of the scaffold with cells compared to simple direct suspension seeding cells that typically leads to non-uniform distribution.[68]
- **The 0.5% collagen seeding method was the most effective overall**: Based on both quantitative metrics and qualitative assessment, the collagen-assisted seeding emerged as the top-performing strategy. Scaffolds seeded with the collagen gel had the highest cell coverage across the scaffold, excellent initial cell viability, and cells that began to interact with the matrix (spreading along collagen fibers and scaffold surfaces). By comparison, the alginate method, while vastly improving uniformity and cell retention relative to suspension, provided a more inert environment, cells were evenly distributed but largely spherical and isolated. The suspension (media) seeding was the least favorable, as many interior regions

had few or no cells and cells tended to aggregate where they were initially dropped. Thus, in answer to our research question, the collagen matrix seeding proved to be the most effective seeding strategy for ensuring a well-populated and biologically supportive scaffold. This results emphasizes the importance of employing natural ECM constituents to seed cells into synthetic scaffolds, a trend promoted by past studies.[35,36] By combining the mechanical strength of PLA with the biological compatibility of collagen, we developed a hybrid system that promoted cell distribution in an optimal manner.

- **The pivotal role of Machine learning and advanced microscopy:** A key aspect of this work was the use of THUNDER microscope imaging coupled with machine learning analysis to rigorously evaluate outcomes. The THUNDER system allowed us to visualize cells deep inside the scaffold with clarity, yielding a rich set of quantitative features per cell/particle. The Random Forest model, trained on these features, could distinguish between the seeding methods with nearly 90% accuracy – essentially “profiling” each seeding condition by its cellular feature signature. This such high precision not only confirmed that the inter-group differences were significant and consistent, but also demonstrates how machine learning could be utilized as an objective assessment tool in tissue engineering. Utilizing SHAP explain-ability further ensured that we could rely and comprehend the model's decision criteria, which aligned with intuitive biological differences (e.g., disparities between groups in the intensity of fluorescence and cell position). Briefly, the application of computational imaging and AI enabled us to extract more from the experiments than would otherwise have been achieved through observation alone; highlighting cell-level subtleties and multi-feature trends typical of each seeding process. This demonstrates the power of combining modern microscopy with machine learning to advance tissue engineering research.[44,49]

Overall, this thesis is a robust demonstration that cell seeding strategy is a predominant factor in the success of scaffold colonization and positions collagen-assisted seeding as an ideal technique for cell integration into 3D bone scaffolds. The discovery is of significance in tissue engineering: by achieving cells to be viably and evenly distributed at the seeding stage, subsequent tissue growth (e.g., osteogenic matrix deposition) will

probably be more uniform and significant. Furthermore, this project provides a framework for using data-driven techniques for evaluating and optimizing bioengineering processes. Future studies can build on these results in the following meaningful ways:

- **Long-term tissue formation and function:** While this study tackled cell distribution and viability in early stages, follow-up studies should determine how such seeding differences translate into more long-term outcomes. For example, one could culture the scaffolds for a few weeks to quantify parameters such as deposition of new bone matrix, mineralization, or expression of osteogenic markers across groups. This would indicate if the collagen-seeded scaffolds not only have more cells initially, but also create faster or more tissue regeneration than the others. The in-vivo test could be the last test, seeding scaffolds differently and placing them inside an animal model to determine which is optimal for healing bone.
- **Scaling and generalization:** We employed a specific scaffold geometry and pore size specific to trabecular bone. It would be interesting to determine whether the advantage of collagen or hydrogel seeding is transferable to other scaffold geometries and compositions. How the pore sizes or architectures interact with one another can arguably be extremely complicated with seeding approaches, i.e., extremely small pores might constrain even cells that are being encapsulated in hydrogel to enter. Thus, studying a range of scaffold designs (for example, with larger sizes or materials such as ceramics or composite polymers) under these seeding regimes will increase our findings' generalizability. Similarly, taking other cell types (such as human mesenchymal stem cells or primary osteoblasts instead of any model cell line) would render the findings generalizable to all clinical tissue engineering situations.
- **Optimization of the hydrogel carriers:** Our results further provoke the optimization of the hydrogel matrices used for seeding. For alginate, one might attempt methods like incorporating RGD peptides or mixing alginate with a low level of collagen or fibrin to give encapsulated cells more opportunities for attachment and communication, perhaps combining the even distribution of alginate with the bioactivity of native ECM.[41,42] For collagen, the modulation of its

concentration or density of cross-linking can control to what extent it stays in the scaffold and scaffolded cells (too high concentration of collagen could reduce cell migration or nutrient diffusion; too low could result in low retention of cells). Other gel systems, including fibrin or gelatin methacrylate (GelMA), can also be investigated that can be made tunable and have on-demand curing for ease. The goal of such technologies would be further improving cell seeding efficiency, viability, and thereby tissue yield.

- **Dynamic seeding and culture methods:** While this study focused exclusively on samples cultured under static conditions, the broader experimental setup also included perfusion-based dynamic culture (without analysis in the current work). Future studies could investigate dynamic seeding strategies in combination with hydrogels, for example, using perfusion to actively draw cell-laden hydrogels into scaffold pores or employing bioprinting techniques for more precise cell placement. It would be intriguing to contrast "hydrogel + perfusion seeding" with pure hydrogel seeding to ascertain whether dynamic flow improves cell uniformity and infiltration into scaffold microstructures. The time of flow commencement (e.g., post-hydrogel gelation vs seeding) may potentially affect cell dispersion and vitality. Optimizing both seeding and dynamic culture conditions will be a key step toward enhancing tissue development in vitro.

- **Machine learning for predictive modeling:** Following the effective use of Random Forest and SHAP in this work, further research may employ more sophisticated AI methodologies to further enhance scaffold design and analysis. For example, convolutional neural networks and other deep learning networks may be trained on images to find patterns in cell distribution or even estimate the seeding strategy without needing to manually extract features. Such models might learn subtle textural or spatial cues beyond the standard morphological features we used. Moreover, ML models could be developed to predict outcomes, e.g., using initial post-seeding imaging to forecast the amount of tissue that will form after a certain culture period. This would allow rapid iteration; different seeding methods or scaffold designs could be screened via imaging and ML prediction,

without waiting weeks for full tissue maturation each time. In line with this, creating user-friendly software tools that incorporate our imaging-analysis pipeline could help other researchers or clinicians quickly evaluate scaffold seeding efficacy in real-time. As noted in a recent review, the incorporation of machine learning in tissue engineering is still expanding, with immense potential to accelerate discovery and optimize protocols.[49] Our study serves as a proof-of-concept for how quantitative microscopy data can be integrated with ML to yield translational insights, and we envision future studies taking this further – for example, by employing live-cell imaging and real-time ML analysis to adjust seeding in real time in a bioreactor (an approach that could ensure every scaffold is seeded to an ideal density before implantation).

In conclusion, the work presented in this thesis contributes both practical knowledge and methodological innovation to the field of bone tissue engineering. We identified a clear winner in terms of seeding strategy which was delivering cells in a collagen hydrogel matrix that significantly improves the uniformity and quality of cell seeding in a 3D printed bone scaffold. This result has the potential to directly impact tissue engineering technique. It is recommended that hybrid scaffold geometries or other hydrogel seeding strategies be implemented when developing large tissue scaffolds to ensure that cells occupy all regions. Moreover, we established a precedent for a data-driven approach to enhance tissue engineering strategies by utilizing sophisticated imaging and machine learning algorithms. The combination of bio-fabrication, imaging, and AI is a powerful approach. It enables scientists to more precisely interpret complex biological outcomes and translate that knowledge to protocol development and scaffold design. Looking forward, the lessons learned here – pertaining to the benefits of homogeneous cell distribution, the usefulness of bioactive seeding carriers, and the necessity for quantitative analysis – form a strong foundation for future projects aimed at engineering functional bone tissue and other regenerative constructs. With continued interdisciplinary effort, involving materials design and computational modeling, we are one step closer to the long-term goal of routinely creating living, functional bone grafts in vitro with the ability to repair or replace flawed bone in vivo. The encouraging results of this project are both a model and an

impetus for such future investigations, one step closer to clinically significant solutions in bone regeneration.[68]

6.Summary

This thesis evaluated the performance of three cell-seeding techniques — cell medium suspension, 2% alginate hydrogel, and 0.5% collagen hydrogel — on 3D-printed PLA scaffolds mimicking trabecular bone. Although both static and perfusion-based dynamic culture conditions were used in the experimental setup, all data analysis and results presented in this thesis were based on scaffolds cultured under static conditions.

High-resolution fluorescence images of cell-seeded scaffolds were recorded with the THUNDER Imager system. Quantitative image analysis was then performed to acquire informative features in terms of morphology, intensity, and position of cells. These data were then analyzed through machine learning programs, Random Forest, to identify the significant parameters to differentiate among the seeding methods.

The research found that seeding with collagen revealed the most uniform cell distribution, whereas suspension offered the most variable and the least uniform staining. The minimum fluorescence intensity and centroid position along Z were the most significant predictors of efficiency of seeding.

In nutshell, the research demonstrates that hydrogel-assisted seeding protocols, specifically collagen, enhance cellular homogeneity and viability in PLA scaffolds under static conditions. Integration of quantitative imaging and machine learning enabled objective assessment of seeding performance, offering a great tool for scaffold design optimization in tissue engineering applications.

7.Bibliography

1. Ma, P.X. (2004). Scaffolds for tissue fabrication. Mater. Today *7*, 30–40. https://doi.org/https://doi.org/10.1016/S1369-7021(04)00233-0.
2. Hutmacher, D.W. (2000). Scaffolds in tissue engineering bone and cartilage. Biomaterials *21*, 2529–2543. https://doi.org/https://doi.org/10.1016/S0142-9612(00)00121-6.
3. Hutmacher, D.W., and Cool, S. (2007). Concepts of scaffold-based tissue engineering—the rationale to use solid free-form fabrication techniques. J. Cell. Mol. Med. *11*, 654–669. https://doi.org/https://doi.org/10.1111/j.1582-4934.2007.00078.x.
4. Billiet, T., Vandenhaute, M., Schelfhout, J., Van Vlierberghe, S., and Dubruel, P. (2012). A review of trends and limitations in hydrogel-rapid prototyping for tissue engineering. Biomaterials *33*, 6020–6041. https://doi.org/https://doi.org/10.1016/j.biomaterials.2012.04.050.
5. Choi, S.-W., Xie, J., and Xia, Y. (2009). Chitosan-Based Inverse Opals: Three-Dimensional Scaffolds with Uniform Pore Structures for Cell Culture. Adv. Mater. *21*, 2997–3001. https://doi.org/https://doi.org/10.1002/adma.200803504.
6. Nseir, N., Regev, O., Kaully, T., Blumenthal, J., Levenberg, S., and Zussman, E. (2012). Biodegradable Scaffold Fabricated of Electrospun Albumin Fibers: Mechanical and Biological Characterization. Tissue Eng. Part C Methods *19*, 257–264. https://doi.org/10.1089/ten.tec.2012.0118.
7. Lohfeld, S., Cahill, S., Barron, V., McHugh, P., Dürselen, L., Kreja, L., Bausewein, C., and Ignatius, A. (2012). Fabrication, mechanical and in vivo performance of polycaprolactone/tricalcium phosphate composite scaffolds. Acta Biomater. *8*, 3446–3456. https://doi.org/https://doi.org/10.1016/j.actbio.2012.05.018.
8. Santos, M.I., Pashkuleva, I., Alves, C.M., Gomes, M.E., Fuchs, S., Unger, R.E.,

Reis, R.L., and Kirkpatrick, C.J. (2009). Surface-modified 3D starch-based scaffold for improved endothelialization for bone tissue engineering. J. Mater. Chem. *19*, 4091–4101. https://doi.org/10.1039/B819089E.

9. Muschler, G.F., Nakamoto, C., and Griffith, L.G. (2004). Engineering Principles of Clinical Cell-Based Tissue Engineering. JBJS *86*.
10. Gao, Y., Lalevée, J., and Simon-Masseron, A. (2023). An Overview on 3D Printing of Structured Porous Materials and Their Applications. Adv. Mater. Technol. *8*, 2300377. https://doi.org/https://doi.org/10.1002/admt.202300377.
11. Guo, Z., and Zhou, C. (2021). Recent advances in ink-based additive manufacturing for porous structures. Addit. Manuf. *48*, 102405. https://doi.org/https://doi.org/10.1016/j.addma.2021.102405.
12. Prem Ananth, K., and Jayram, N.D. (2024). A comprehensive review of 3D printing techniques for biomaterial-based scaffold fabrication in bone tissue engineering. Ann. 3D Print. Med. *13*, 100141. https://doi.org/https://doi.org/10.1016/j.stlm.2023.100141.
13. Chia, H.N., and Wu, B.M. (2015). Recent advances in 3D printing of biomaterials. J. Biol. Eng. *9*, 4. https://doi.org/10.1186/s13036-015-0001-4.
14. Szymczyk-Ziółkowska, P., Łabowska, M.B., Detyna, J., Michalak, I., and Gruber, P. (2020). A review of fabrication polymer scaffolds for biomedical applications using additive manufacturing techniques. Biocybern. Biomed. Eng. *40*, 624–638. https://doi.org/https://doi.org/10.1016/j.bbe.2020.01.015.
15. Mazzanti, V., Malagutti, L., and Mollica, F. (2019). FDM 3D Printing of Polymers Containing Natural Fillers: A Review of their Mechanical Properties, https://doi.org/10.3390/polym11071094 https://doi.org/10.3390/polym11071094.
16. Le Duigou, A., Chabaud, G., Matsuzaki, R., and Castro, M. (2020). Tailoring the mechanical properties of 3D-printed continuous flax/PLA biocomposites by controlling the slicing parameters. Compos. Part B Eng. *203*, 108474. https://doi.org/https://doi.org/10.1016/j.compositesb.2020.108474.
17. Wüst, S., Müller, R., and Hofmann, S. (2011). Controlled Positioning of Cells in Biomaterials—Approaches Towards 3D Tissue Printing, https://doi.org/10.3390/jfb2030119 https://doi.org/10.3390/jfb2030119.

18. Xia, H., Zhao, D., Zhu, H., Hua, Y., Xiao, K., Xu, Y., Liu, Y., Chen, W., Liu, Y., Zhang, W., et al. (2018). Lyophilized Scaffolds Fabricated from 3D-Printed Photocurable Natural Hydrogel for Cartilage Regeneration. ACS Appl. Mater. Interfaces *10*, 31704–31715. https://doi.org/10.1021/acsami.8b10926.
19. Markovic, M., Van Hoorick, J., Hölzl, K., Tromayer, M., Gruber, P., Nürnberger, S., Dubruel, P., Van Vlierberghe, S., Liska, R., and Ovsianikov, A. (2015). Hybrid Tissue Engineering Scaffolds by Combination of Three-Dimensional Printing and Cell Photoencapsulation. J. Nanotechnol. Eng. Med. *6*. https://doi.org/10.1115/1.4031466.
20. Kumar, A., Nune, K.C., and Misra, R.D.K. (2016). Biological functionality of extracellular matrix-ornamented three-dimensional printed hydroxyapatite scaffolds. J. Biomed. Mater. Res. Part A *104*, 1343–1351. https://doi.org/https://doi.org/10.1002/jbm.a.35664.
21. Dutta, R.C., and Dutta, A.K. (2009). Cell-interactive 3D-scaffold; advances and applications. Biotechnol. Adv. *27*, 334–339. https://doi.org/https://doi.org/10.1016/j.biotechadv.2009.02.002.
22. Kim, Y., Ko, H., Kwon, I.K., and Shin, K. (2016). Extracellular Matrix Revisited: Roles in Tissue Engineering. Int Neurourol J *20*, S23-29. https://doi.org/10.5213/inj.1632600.318.
23. Gilpin, A., and Yang, Y. (2017). Decellularization Strategies for Regenerative Medicine: From Processing Techniques to Applications. Biomed Res. Int. *2017*, 9831534. https://doi.org/https://doi.org/10.1155/2017/9831534.
24. Jun, I., Han, H.-S., Edwards, J.R., and Jeon, H. (2018). Electrospun Fibrous Scaffolds for Tissue Engineering: Viewpoints on Architecture and Fabrication, https://doi.org/10.3390/ijms19030745 https://doi.org/10.3390/ijms19030745.
25. Bittner, S.M., Guo, J.L., Melchiorri, A., and Mikos, A.G. (2018). Three-dimensional printing of multilayered tissue engineering scaffolds. Mater. Today *21*, 861–874. https://doi.org/https://doi.org/10.1016/j.mattod.2018.02.006.
26. Jenkins, T.L., and Little, D. (2019). Synthetic scaffolds for musculoskeletal tissue engineering: cellular responses to fiber parameters. npj Regen. Med. *4*, 15. https://doi.org/10.1038/s41536-019-0076-5.

27. Zhu, N., and Chen, X. (2013). Biofabrication of Tissue Scaffolds. In, R. Pignatello, ed. (IntechOpen), p. Ch. 12. https://doi.org/10.5772/54125.
28. Grémare, A., Guduric, V., Bareille, R., Heroguez, V., Latour, S., L'heureux, N., Fricain, J.-C., Catros, S., and Le Nihouannen, D. (2018). Characterization of printed PLA scaffolds for bone tissue engineering. J. Biomed. Mater. Res. Part A *106*, 887–894. https://doi.org/https://doi.org/10.1002/jbm.a.36289.
29. Gunatillake, P. (2003). Biodegradable synthetic polymers for tissue engineering. Eur. Cells Mater. *5*, 1–16. https://doi.org/10.22203/eCM.v005a01.
30. Dong, C., and Lv, Y. (2016). Application of Collagen Scaffold in Tissue Engineering: Recent Advances and New Perspectives, https://doi.org/10.3390/polym8020042 https://doi.org/10.3390/polym8020042.
31. Le Bao Ha, T., Quan, T.M., Nguyen Vu, D., and Minh Si, D. (2013). Naturally Derived Biomaterials: Preparation and Application. In, J. A. Andrades, ed. (IntechOpen). https://doi.org/10.5772/55668.
32. Ahn, S., Kim, Y., Lee, H., and Kim, G. (2012). A new hybrid scaffold constructed of solid freeform-fabricated PCL struts and collagen struts for bone tissue regeneration: fabrication, mechanical properties, and cellular activity. J. Mater. Chem. *22*, 15901–15909. https://doi.org/10.1039/C2JM33310D.
33. Huang, S., and Fu, X. (2010). Naturally derived materials-based cell and drug delivery systems in skin regeneration. J. Control. Release *142*, 149–159. https://doi.org/https://doi.org/10.1016/j.jconrel.2009.10.018.
34. Martin, R.B., Burr, D.B., and Sharkey, N.A. (1998). Skeletal Tissue Mechanics (Springer New York) https://doi.org/10.1007/978-1-4757-2968-9.
35. Glowacki, J., and Mizuno, S. (2008). Collagen scaffolds for tissue engineering. Biopolymers *89*, 338–344. https://doi.org/https://doi.org/10.1002/bip.20871.
36. Kim, G., Ahn, S., Kim, Y., Cho, Y., and Chun, W. (2011). Coaxial structured collagen–alginate scaffolds: fabrication, physical properties, and biomedical application for skin tissue regeneration. J. Mater. Chem. *21*, 6165–6172. https://doi.org/10.1039/C0JM03452E.
37. Gombotz, W.R., and Wee, S. (1998). Protein release from alginate matrices. Adv. Drug Deliv. Rev. *31*, 267–285. https://doi.org/https://doi.org/10.1016/S0169-

409X(97)00124-5.

38. Kim, W.S., Mooney, D.J., Arany, P.R., Lee, K., Huebsch, N., and Kim, J. (2011). Adipose Tissue Engineering Using Injectable, Oxidized Alginate Hydrogels. Tissue Eng. Part A *18*, 737–743. https://doi.org/10.1089/ten.tea.2011.0250.
39. Suzuki, Y., Nishimura, Y., Tanihara, M., Suzuki, K., Nakamura, T., Shimizu, Y., Yamawaki, Y., and Kakimaru, Y. (1998). Evaluation of a novel alginate gel dressing: Cytotoxicity to fibroblasts in vitro and foreign-body reaction in pig skin in vivo. J. Biomed. Mater. Res. *39*, 317–322. https://doi.org/https://doi.org/10.1002/(SICI)1097-4636(199802)39:2<317::AID-JBM20>3.0.CO;2-8.
40. Peters, M.C., Polverini, P.J., and Mooney, D.J. (2002). Engineering vascular networks in porous polymer matrices. J. Biomed. Mater. Res. *60*, 668–678. https://doi.org/https://doi.org/10.1002/jbm.10134.
41. Lee, K.Y., and Mooney, D.J. (2012). Alginate: Properties and biomedical applications. Prog. Polym. Sci. *37*, 106–126. https://doi.org/https://doi.org/10.1016/j.progpolymsci.2011.06.003.
42. Neves, M.I., Moroni, L., and Barrias, C.C. (2020). Modulating Alginate Hydrogels for Improved Biological Performance as Cellular 3D Microenvironments. Front. Bioeng. Biotechnol. *8*.
43. Jovel, J., and Greiner, R. (2021). An Introduction to Machine Learning Approaches for Biomedical Research. Front. Med. *Volume 8*-.
44. Sun, J., Yao, K., Huang, K., and Huang, D. (2022). Machine learning applications in scaffold based bioprinting. Mater. Today Proc. *70*, 17–23. https://doi.org/https://doi.org/10.1016/j.matpr.2022.08.485.
45. Orange Data Mining https://orangedatamining.com.
46. Orange - Feature Selection https://oldorange.biolab.si/workflows/Feature-Selection/#:~:text=For supervised problems%2C where data,and display its scatter plot.
47. Python https://www.python.org/.
48. Omigbodun, F.T., Osa-Uwagboe, N., Udu, A.G., and Oladapo, B.I. (2024). Leveraging Machine Learning for Optimized Mechanical Properties and 3D Printing

of PLA/cHAP for Bone Implant, https://doi.org/10.3390/biomimetics9100587 https://doi.org/10.3390/biomimetics9100587.

49. Jeznach, O., Tabakoglu, S., Zaszczyńska, A., and Sajkiewicz, P. (2024). Review on machine learning application in tissue engineering: What has been done so far? Application areas, challenges, and perspectives. J. Mater. Sci. *59*, 21222–21250. https://doi.org/10.1007/s10853-024-10449-2.
50. Conev, A., Litsa, E.E., Perez, M.R., Diba, M., Mikos, A.G., and Kavraki, L.E. (2020). Machine Learning-Guided Three-Dimensional Printing of Tissue Engineering Scaffolds. Tissue Eng. Part A *26*, 1359–1368. https://doi.org/10.1089/ten.tea.2020.0191.
51. Wu, Y., Ding, X., Wang, Y., and Ouyang, D. (2024). Harnessing the power of machine learning into tissue engineering: current progress and future prospects. Burn. Trauma *12*, tkae053. https://doi.org/10.1093/burnst/tkae053.
52. Menon, A., Póczos, B., Feinberg, A.W., and Washburn, N.R. (2019). Optimization of Silicone 3D Printing with Hierarchical Machine Learning. 3D Print. Addit. Manuf. *6*, 181–189. https://doi.org/10.1089/3dp.2018.0088.
53. Jin, Z., Zhang, Z., and Gu, G.X. (2020). Automated Real-Time Detection and Prediction of Interlayer Imperfections in Additive Manufacturing Processes Using Artificial Intelligence. Adv. Intell. Syst. *2*, 1900130. https://doi.org/https://doi.org/10.1002/aisy.201900130.
54. Jin, Z., Zhang, Z., and Gu, G.X. (2019). Autonomous in-situ correction of fused deposition modeling printers using computer vision and deep learning. Manuf. Lett. *22*, 11–15. https://doi.org/https://doi.org/10.1016/j.mfglet.2019.09.005.
55. Gu, G.X., Chen, C.-T., Richmond, D.J., and Buehler, M.J. (2018). Bioinspired hierarchical composite design using machine learning: simulation, additive manufacturing, and experiment. Mater. Horizons *5*, 939–945. https://doi.org/10.1039/C8MH00653A.
56. Abueidda, D.W., Almasri, M., Ammourah, R., Ravaioli, U., Jasiuk, I.M., and Sobh, N.A. (2019). Prediction and optimization of mechanical properties of composites using convolutional neural networks. Compos. Struct. *227*, 111264. https://doi.org/https://doi.org/10.1016/j.compstruct.2019.111264.

57. Silbernagel, C., Aremu, A., and Ashcroft, I. (2020). Using machine learning to aid in the parameter optimisation process for metal-based additive manufacturing. Rapid Prototyp. J. *26*, 625–637. https://doi.org/10.1108/RPJ-08-2019-0213.
58. Pecci, R., Baiguera, S., Ioppolo, P., Bedini, R., and Del Gaudio, C. (2020). 3D printed scaffolds with random microarchitecture for bone tissue engineering applications: Manufacturing and characterization. J. Mech. Behav. Biomed. Mater. *103*, 103583. https://doi.org/https://doi.org/10.1016/j.jmbbm.2019.103583.
59. Ledda, M., Merco, M., Sciortino, A., Scatena, E., Convertino, A., Lisi, A., and Del Gaudio, C. (2022). Biological Response to Bioinspired Microporous 3D-Printed Scaffolds for Bone Tissue Engineering, https://doi.org/10.3390/ijms23105383 https://doi.org/10.3390/ijms23105383.
60. Gabetti, S., Masante, B., Schiavi, A., Scatena, E., Zenobi, E., Israel, S., Sanginario, A., Del Gaudio, C., Audenino, A., Morbiducci, U., et al. (2024). Adaptable test bench for ASTM-compliant permeability measurement of porous scaffolds for tissue engineering. Sci. Rep. *14*, 1722. https://doi.org/10.1038/s41598-024-52159-4.
61. Gabetti, S., Masante, B., Cochis, A., Putame, G., Sanginario, A., Armando, I., Fiume, E., Scalia, A.C., Daou, F., Baino, F., et al. (2022). An automated 3D-printed perfusion bioreactor combinable with pulsed electromagnetic field stimulators for bone tissue investigations. Sci. Rep. *12*, 13859. https://doi.org/10.1038/s41598-022-18075-1.
62. Bancroft, G.N., Sikavitsas, V.I., van den Dolder, J., Sheffield, T.L., Ambrose, C.G., Jansen, J.A., and Mikos, A.G. (2002). Fluid flow increases mineralized matrix deposition in 3D perfusion culture of marrow stromal osteoblasts in a dose-dependent manner. Proc. Natl. Acad. Sci. *99*, 12600–12605. https://doi.org/10.1073/pnas.202296599.
63. Wittkowske, C., Reilly, G.C., Lacroix, D., and Perrault, C.M. (2016). In Vitro Bone Cell Models: Impact of Fluid Shear Stress on Bone Formation. Front. Bioeng. Biotechnol. *4*.
64. James, S., Fox, J., Afsari, F., Lee, J., Clough, S., Knight, C., Ashmore, J., Ashton, P., Preham, O., Hoogduijn, M., et al. (2015). Multiparameter Analysis of Human Bone Marrow Stromal Cells Identifies Distinct Immunomodulatory and

Differentiation-Competent Subtypes. Stem Cell Reports *4*, 1004–1015. https://doi.org/10.1016/j.stemcr.2015.05.005.

65. Thunder Imaging Systems https://www.leica-microsystems.com/products/thunder-imaging-systems/.
66. Leica Microsystems https://www.leica-microsystems.com/science-lab/life-science/an-introduction-to-computational-clearing/.
67. THUNDER Imagers: High Performance, Versatility and Ease-of-Use for your Everyday Imaging Workflows https://www.leica-microsystems.com/science-lab/life-science/thunder-imagers-high-performance-versatility-and-ease-of-use-for-your-everyday-imaging-workflows/.
68. Chan, B.P., and Leong, K.W. (2008). Scaffolding in tissue engineering: general approaches and tissue-specific considerations. Eur. Spine J. *17*, 467–479. https://doi.org/10.1007/s00586-008-0745-3.
69. Nguyen, K.T., and West, J.L. (2002). Photopolymerizable hydrogels for tissue engineering applications. Biomaterials *23*, 4307–4314. https://doi.org/https://doi.org/10.1016/S0142-9612(02)00175-8.

Appendix

Table 1. ANOVA Results with Bonferroni

Feature	Group 1	Group 2	Mean Difference	p-value raw	Reject H0 (Uncorrected)	p-value Bonferroni	Significant (Bonferroni)
Convex Surface Area [micrometers²]	Alginate	Collagen	0.0053	0.0621	False	1.0	False
Convex Surface Area [micrometers²]	Alginate	Media	0.1026	0.161	False	1.0	False
Convex Surface Area [micrometers²]	Collagen	Media	0.0973	0.1934	False	1.0	False
Sphericity	Alginate	Collagen	0.0318	0.0001	True	0.0045000000000000005	True
Sphericity	Alginate	Media	-0.3186	0.1791	False	1.0	False
Sphericity	Collagen	Media	-0.3504	0.1253	False	1.0	False
Diameter [micrometers]	Alginate	Collagen	0.0242	0.0	True	0.0	True
Diameter [micrometers]	Alginate	Media	0.2907	0.027	True	1.0	False
Diameter [micrometers]	Collagen	Media	0.2665	0.0478	True	1.0	False
Ellipsoid Major [micrometers]	Alginate	Collagen	0.0322	0.0	True	0.0	True
Ellipsoid Major [micrometers]	Alginate	Media	0.4922	0.0	True	0.0	True
Ellipsoid Major [micrometers]	Collagen	Media	0.46	0.0	True	0.0	True
Ellipsoid Minor [micrometers]	Alginate	Collagen	0.0123	0.0	True	0.0	True
Ellipsoid Minor [micrometers]	Alginate	Media	0.1533	0.0523	False	1.0	False
Ellipsoid Minor [micrometers]	Collagen	Media	0.141	0.0822	False	1.0	False
Feret Maximum [micrometers]	Alginate	Collagen	0.0409	0.0	True	0.0	True
Feret Maximum [micrometers]	Alginate	Media	0.6454	0.0	True	0.0	True
Feret Maximum [micrometers]	Collagen	Media	0.6045	0.0	True	0.0	True
Feret Maximum Elevation [°]	Alginate	Collagen	0.0794	0.0096	True	0.43199999999999994	False
Feret Maximum Elevation [°]	Alginate	Media	-0.805	0.4274	False	1.0	False
Feret Maximum Elevation [°]	Collagen	Media	-0.8844	0.3587	False	1.0	False
Feret Minimum [micrometers]	Alginate	Collagen	0.0128	0.0001	True	0.0045000000000000005	True
Feret Minimum [micrometers]	Alginate	Media	0.1918	0.0213	True	0.9585	False
Feret Minimum [micrometers]	Collagen	Media	0.179	0.0348	True	1.0	False

Feret Ratio	Alginate	Collagen	-0.0158	0.0274	True	1.0	False
Feret Ratio	Alginate	Media	-0.1123	0.7252	False	1.0	False
Feret Ratio	Collagen	Media	-0.0965	0.789	False	1.0	False
Centroid Z [micrometers]	Alginate	Collagen	0.4502	0.0	True	0.0	True
Centroid Z [micrometers]	Alginate	Media	-0.0896	0.9491	False	1.0	False
Centroid Z [micrometers]	Collagen	Media	-0.5398	0.1521	False	1.0	False
Bounds Z [micrometers]	Alginate	Collagen	0.0497	0.0	True	0.0	True
Bounds Z [micrometers]	Alginate	Media	0.7538	0.0	True	0.0	True
Bounds Z [micrometers]	Collagen	Media	0.704	0.0	True	0.0	True
Intensity Mean	Alginate	Collagen	-0.1809	0.0	True	0.0	True
Intensity Mean	Alginate	Media	-0.6734	0.0003	True	0.013499999999999998	True
Intensity Mean	Collagen	Media	-0.4925	0.0124	True	0.5579999999999999	False
Intensity Standard Deviation	Alginate	Collagen	-0.0016	0.9823	False	1.0	False
Intensity Standard Deviation	Alginate	Media	1.3992	0.0	True	0.0	True
Intensity Standard Deviation	Collagen	Media	1.4008	0.0	True	0.0	True
Intensity Minimum	Alginate	Collagen	-0.2264	0.0	True	0.0	True
Intensity Minimum	Alginate	Media	-1.789	0.0	True	0.0	True
Intensity Minimum	Collagen	Media	-1.5625	0.0	True	0.0	True
Intensity Maximum	Alginate	Collagen	-0.0837	0.0	True	0.0	True
Intensity Maximum	Alginate	Media	0.9248	0.0049	True	0.2205	False
Intensity Maximum	Collagen	Media	1.0085	0.0018	True	0.081	False